The hidden monzogranite of Soultz-sous-Forêts (Rhine Graben, France).
Mineralogy, petrology and genesis *

Jean-Marc STUSSI [1]
Alain CHEILLETZ [2, 3]
Jean-Jacques ROYER [2, 3]
Philippe CHÈVREMONT [4]
Gilbert FÉRAUD [5]

*Le monzogranite sous couverture de Soultz-sous-Forêts (graben rhénan, France).
Minéralogie, pétrologie et genèse*

Abstract

Drilling at Soultz-sous-Forêts, France, conducted as part of the European Hot Dry Rock (HDR) Project, penetrated granitic basement down to 5,080 m and revealed a porphyritic monzogranite that has no known equivalent in the granitic outcrops of adjacent basement areas. The EPS-1 borehole core (from 980 to 2,230 m) shows a monzogranite that has a high-K calc-alkaline composition and is enriched in K, Th, U, and REE. Petrological and mineralogical characteristics indicate that the monzogranite formed through two crystallization stages: a first, deep-seated, stage was characterized by the crystallization of liquidus phases in the 755-790 °C range, at 3.5 kb (11-12 km depth). This was followed, during ascent and at emplacement level, by consolidation at 665-715 °C, 1.5-2.0 kb (4.5-5.5 km depth) associated with the development of K-feldspar layering. Published Rb/Sr ages (325 Ma), new $^{40}Ar/^{39}Ar$ cooling ages (319 Ma), a U/Pb on zircon emplacement age of 331 Ma, and petrological arguments such as the presence of monzogabbrodiorite to quartz-syenite enclaves, indicate that the Soultz monzogranite had a mainly crustal origin with a possible contribution of mantle-derived components represented by the enclaves. Emplacement was related to collision tectonics during the transition between Early and Late Carboniferous.

Résumé

*Retenu comme l'une des cibles du projet Europe Hot Dry Rock (HDR), le socle sous couverture secondaire et tertiaire du site de Soultz-sous-Forêts (graben rhénan, France) a été atteint à 1 430 m, foré en carotté continu jusqu'à 2 230 m (sondage EPS-1) et en destructif jusqu'à 5 080 m (sondage GPK2). Ce socle est constitué d'un monzogranite à méga-cristaux de feldspath potassique dont on ne connaissait pas d'équivalent de surface dans les régions hercyniennes voisines. Les variations des caractéristiques pétrologiques le long de la colonne carottée du monzogranite ont été déterminées à partir du prélèvement de 14 échantillons, ainsi que des analyses effectuées antérieurement par le BRGM (dont 5 enclaves). Le monzogranite de Soultz se caractérise par une paragenèse minérale à quartz, plagioclase, orthose, biotite, amphibole, sphène, alla-*nite et par une composition calco-alcaline potassique, enrichie en Ba, K, Th, U, Y, et terres rares. Les variations chimiques le long du sondage mettent en évidence deux zones ne présentant pas de solution de continuité. Elles se distinguent par les abondances de minéraux (hornblende, biotite, plagioclase, orthose), par les teneurs en Ba, Sr, Th et terres rares (biotite, orthose, Ba Th et terres rares plus élevées en dessous de la cote 1 800 m) et par leurs modalités de variation (plus régulières en profondeur qu'au-dessus de 1 800 m). Ces variations sont rapportées à des fractionnements solide-liquide lors de l'ascension et de la mise en place du monzogranite. À ces variations se superposent des litages magmatiques formés par l'accumulation de mégacristaux de feldspath potassique (jusqu'à 60 % d'orthose) et quelquefois de minéraux ferro-magnésiens. D'après la course de cristallisation des minéraux et les paramètres intensifs obtenus (pression de cristallisation calculée à partir de la composition zonée de la hornblende, température de cristallisation, f_{O2}), le monzogranite aurait cristallisé en deux stades : (i) un stade profond à 3,5 kb (11-12 km) et à 755-790 °C (minéraux au

liquidus : hornblende, rare sphène, alla-nite, biotite, orthose, plagioclase), (2) un stade d'ascension et de mise en place du magma à 1,5-2,0 kb (4,5-5,5 km) et 665-715 °C, marqué par la fin de cristallisation de la hornblende et de la magnétite, déve-loppement du litage magmatique et consolidation de la matrice quartzo-feld-spathique. La mise en place du monzogra-nite est accompagnée d'un magmatisme shoshonitique synchrone représenté par des enclaves de monzogabbrodiorites, monzodiorites quartzifères, monzonites quartzifères et syénites quartzifères forte-ment enrichies en K, Th, U, et terres rares. Les rapports initiaux du strontium ($^{87/86}$Sr = 0.7058), ainsi que les simulations par bilans de masse et fractionnement d'élé-ments traces, il est suggéré que le monzo-granite aurait une origine essentiellement crustale impliquant un constituant mantello-dérivé représenté le plus proba-blement par les monzodiorites quartzifères rencontrées en enclaves.

D'après les datations isotopiques Rb/Sr à 325 Ma, K/Ar (321 ± 8 Ma), ^{40}Ar/^{39}Ar (319,8 ± 0,6 à 322,4 ± 0,4 Ma ; âges de refroidissement) et U/Pb sur zircon (331 ± 9 Ma ; âge de mise en place), le monzogranite s'est mis en place à la limite du Viséen supérieur et du Namurien. Le monzogranite de Soultz constitue de ce fait l'une des dernières manifestations plutoniques actuellement connues dans le domaine de la ride cris-talline médio-germanique. Par ses caractéristiques pétrologiques (Th, U, Y, Zr, terres rares), il s'apparente davantage aux monzogranites shoshonitiques de Senones et Natzwiller (Vosges septentrio-nales) qu'aux granites ultimes de l'unité III de l'Odenwald (Heidelberg, Tromm). L'âge de mise en place et la structure magmatique fruste indiquent pour le monzogranite de Soultz une mise en place syn- à post-D4 par rapport aux phases de déformation de l'Odenwald. Celle-ci s'inscrirait dans un contexte collisionnel à post-collisionnel des zones externes septentrionales de l'orogène varisque centre-ouest européen.

Introduction

The Soultz-sous-Forêts site in the Rhine Graben (Alsace, France) has been selected as one of the three main areas in Europe for demonstrating the feasibility of the Europe Hot Dry Rock (HDR) concept (Bresee, 1992), because of its high geo-thermal gradient (Gérard and Kappelmeyer, 1987) that probably results from the upwelling of hot fluids from depth (Clauser, 1989). It is located along the Rhine Graben where several geothermal anomalies are known. The physical char-acteristics of the heat exchanger have been investigated through structural, mechan-ical, and thermal studies, as well as model-ling based on logging of the three wells GPK1, GPK2 and EPS-1 (Traineau *et al.*,
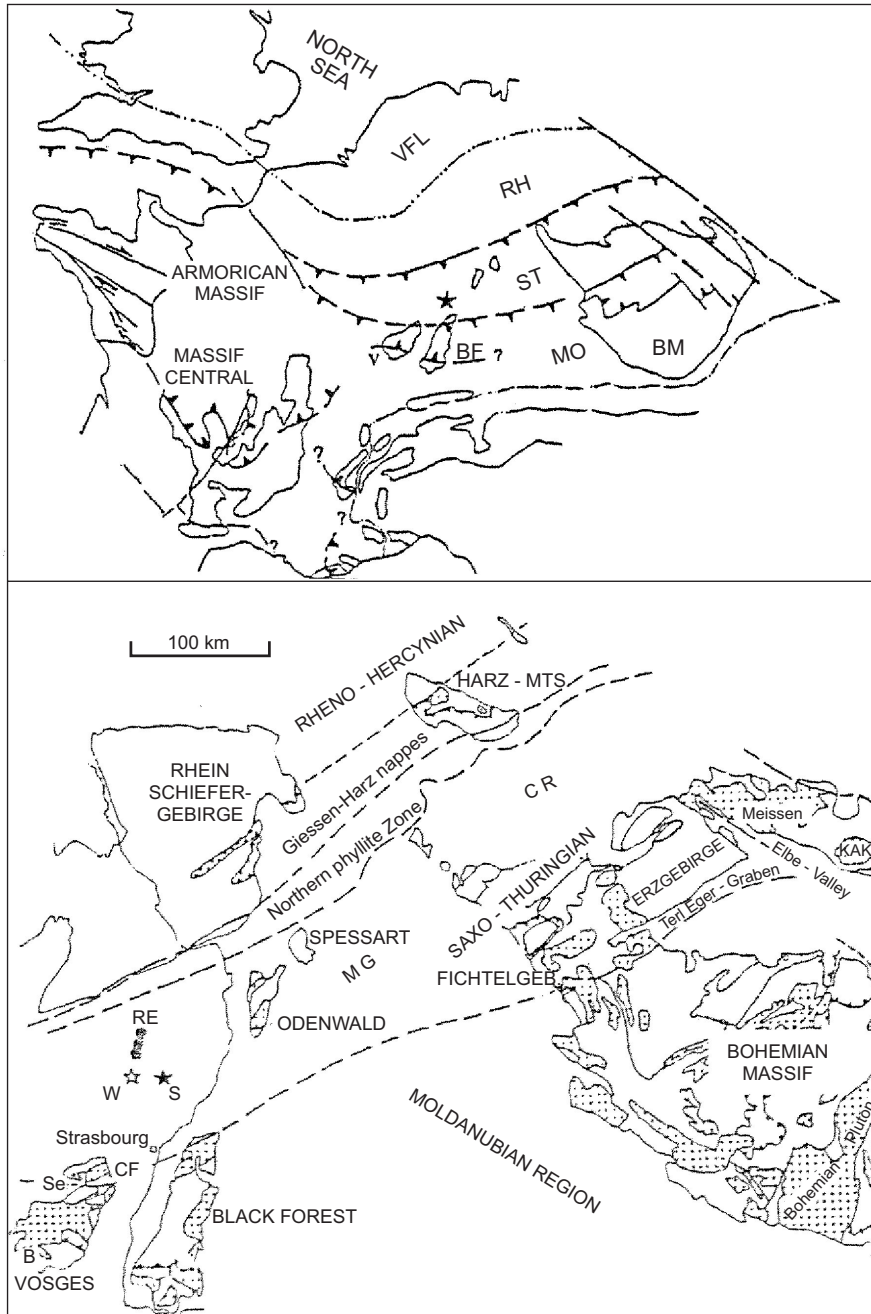
Fig. 1.- Geological sketch map and location of the Soultz monzogranite in the Variscan Saxo-Thuringian zone (after Franke, 1989a, simplified).
Abbreviations: VFL:Variscan Front Line; RH: Rheno-Hercynian zone; ST: Saxo-Thuringian zone; MGCR: Mid-German Crystalline Rise; MO: Moldanubian zone; BM: Bohemian massif; V: Vosges; BF: Black Forest; RE: Rhine Graben escarpment intrusions; W: Windstein; S: Soultz; CF: Champ-du-Feu; Se: Senones; B: Ballons.

Fig. 1.- Le site de Soultz dans son cadre géologique Saxo-Thuringien (d'après Franke (1989a) simplifié). Abréviations : VFL : front varisque ; RH : zone rhéno-hercynienne ; ST : Saxo-Thuringien ; MGCR : Ride cristalline médio-germanique ; MO : Moldanubien ; BM : Massif de Bohême ; BF : Forêt-Noire ; RE : intrusions du talus rhénan occidental. Autres abréviations, cf. légende anglaise.

1991; Genter and Traineau, 1992; Kappelmeyer *et al.*, 1991; Dezayes *et al.*, 1995, 1996; Genter *et al.*, 1995; Schulmann *et al.*, 1997; Ledésert *et al.*, 1999).

The heat exchanger is located within a buried granitoid intrusion of the Variscan basement beneath Mesozoic and Cenozoic rocks in the Rhine Graben. Outcrops of this basement occur in the Odenwald, the Northern Vosges and locally along the Western Rhine Graben escarpment. This study focuses on the petrology, mineralogy and genesis of the blind Soultz monzogranite intrusion. Three deep holes penetrate the basement, GPK-1, GPK-2 and EPS-1. GPK-2 was recently deepened to 5,080 m depth, while GPK-1 reached 3,580 m (Elsass *et al.*, 1995) providing an exceptional cross section through the granitic basement of the Rhine Graben. Only EPS-1 was cored continuously from 980 to 2,230 m; in addition to previous analyses (including five enclaves) by BRGM, 14 new samples collected from this drill-core have been analysed in order to define the origin and emplacement of the Soultz monzogranite. A brief comparison is made with granitoids from other regional intrusions.

Geological setting

The Soultz geothermal site is located in the western part of the Rhine Graben near Soultz-sous-Forêts (40 km NNW from Strasbourg) and 15 km east of the Vosges fault that separates the northern Vosges Variscan basement from the Tertiary graben system (Fig. 1). Borehole EPS-1 is 2230 m deep and reached the porphyritic monzogranite basement at a depth of 1426 m. The petrological features of this basement differ from the nearest outcropping calc-alkaline granodiorite at Windstein, 16 km to the west (Bassahak and Gagny, 1987; Flöttmann and Oncken, 1992), as well as from other granitoids exposed in adjacent basement areas (Western Rhine Graben escarpment, Northern Vosges Senones - Champ-du-Feu plutonic complex, Northern Black Forest, Odenwald). According to the regional structure of the European Variscan, the hidden Soultz monzogranite intrusion belongs to the Saxo-Thuringian Zone, and more precisely to the Mid-German Crystalline Rise (MGCR) (Franke, 1989a, 1989b; Oncken, 1997).
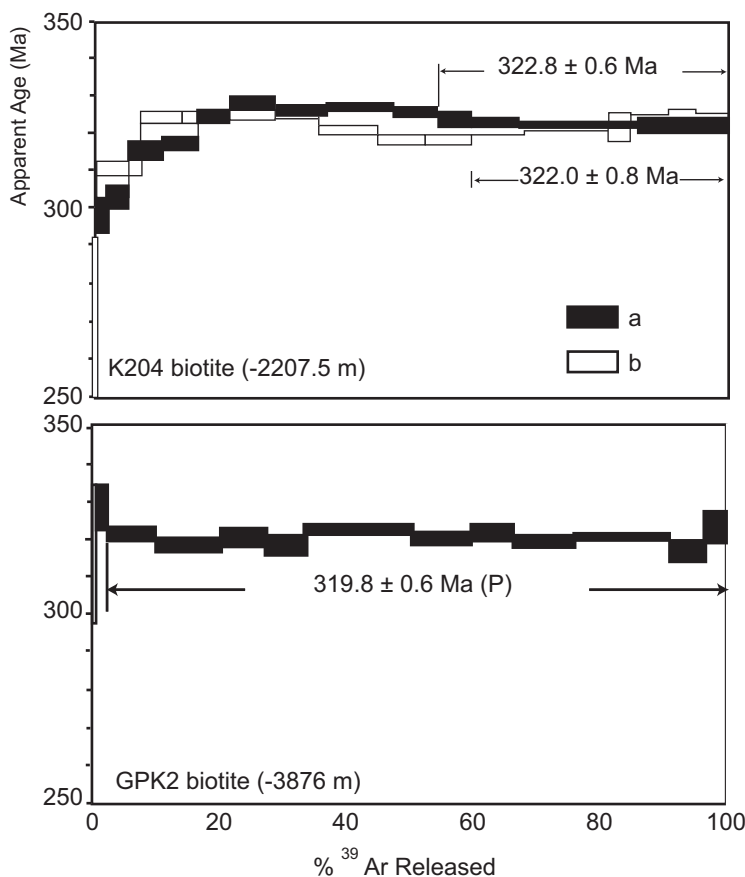

Fig. 2.- $^{40}Ar/^{39}Ar$ age spectra of separated biotites from the Soultz monzogranite. a, b : K2O4 separates a and b.

Fig. 2.- Spectres $^{40}Ar/^{39}Ar$ de biotites séparées du monzogranite de Soultz. a, b : séparations a et b de K2O4.

The Soultz intrusion is unconformably overlain by a Mesozoic sedimentary succession resting on a pre-Liassic erosion surface affecting the basement. According to gravity data, the surface of the pluton is about 100 km^2. Rb/Sr isochrons yield a cooling age of 325 ± 6 Ma (Sr$_i$ = 0.7058; Rummel, 1991), whereas recent U/Pb on zircon dating gave an emplacement age of 331 ± 9 Ma (Alexandrov *et al.*, 2001). This indicates a probable Early Namurian emplacement age (Gradstein and Odd, 1997) associated with a rapid cooling of the Soultz intrusion. The ages are within the range obtained for several granitoid intrusions in adjacent basement areas (Hellman *et al.*, 1982; Boutin *et al.*, 1995; Hess *et al.*, 1995; Reischmann and Anthes, 1996; Altherr *et al.*, 2000).

K-Ar and $^{40}Ar/^{39}Ar$ dating

In order to constrain the cooling evolution of the pluton, K-Ar and $^{40}Ar/^{39}Ar$ dating was done on biotite separates from two samples, K2O4 (EPS-1 well, 2,207 m

depth) and GPK2 (cuttings from GPK2 well, 3,876 m depth). Biotite separates were handpicked under a binocular microscope in the range of 315/500 μm from coarse fractions of the crushed sample K2O4, and in the range of 50/400 μm for the GPK2 cuttings. Biotite separates from sample K2O4 show very slight chlorite alteration estimated below 1% by X-ray analysis. Biotite grains from sample GPK2 are fresh. In the GPK2 well, logging-measurements of K, Th and U content are consistent with the extension of the monzogranite similar to K2O4 from EPS-1 down to 3,876 m.

Two K-Ar determinations on the K2O4 biotite concentrates (Table 1) give ages of 317 ± 8 Ma and 325 ± 8 Ma, which are within the 1σ error bar. The mean age calculated from these two determinations is 321 ± 8 Ma, concordant with the 325 ± 6 Ma Rb/Sr isochron age (Rummel, 1991).

$^{40}Ar/^{39}Ar$ dating on two biotite grains yielded step-heating spectra with distinct

Sample	K$_2$O (wg + %)	^{40}Ar * (10^{15} at/g)	^{40}K (10^{15} at/g)	Age (Ma)	Error (± 1 σ)
Biotite K 204 (1)	8.55	2.57	127.6	317	7
Biotite K 204 (2)	8.55	2.63	127.6	324	7

Table 1.- Analytical data for K/Ar dates of the Soultz monzogranite.

Tabl. 1.- Données analytiques des datations K/Ar du monzogranite de Soultz.

Atmospheric contamination (%)	^{39}Ar	^{40}Ar*/^{39}ArK	Apparent age (Ma)	Error (± 1 σ)
Single grain laser analysis. Sample K 204 Analysis V960. Steps				
1	97.707	0.139	3.98 ± 3.58	124.25	108.39
2	24.302	0.517	4.39 ± 0.44	136.54	13.254
3	6.89	1.682	10.03 ± 0.16	298.45	4.51
4	-2.81	3.203	10.21 ± 0.10	303.29	2.81
5	0.87	5.467	10.67 ± 0.07	315.94	2.04
6	1.37	5.699	10.73 ± 0.06	317.57	1.86
7	0.11	5.146	11.01 ± 0.05	325.06	1.51
8	-	6.944	11.12 ± 0.05	328.04	1.57
9	0.64	8.339	11.07 ± 0.04	326.53	1.31
10	-	10.22	11.09 ± 0.04	327.28	1.07
11	-	6.622	11.03 ± 0.04	325.71	1.31
12	-	5.314	10.96 ± 0.07	323.76	1.94
13	0.02	7.732	10.94 ± 0.04	323.09	1.27
14	-	18.501	10.91 ± 0.02	322.36	0.63
15	-	6.87	10.93 ± 0.04	322.75	1.3
16	-	7.606	10.94 ± 0.04	323.05	1.3

Integrated age = 321.4 ± 0.4 Ma
Plateau age (steps 12-16) = 322.8 ± 0.6 Ma (1 σ)

Atmospheric contamination (%)	^{39}Ar	^{40}Ar*/^{39}ArK	Apparent age (Ma)	Error (± 1 σ)
Single grain laser analysis. Sample GPK2. Analysis V 1021. Steps				
1	3.86	0.739	9.22 ± 0.60	275.99	16.51
2	1.21	6.701	10.48 ± 0.07	310.83	1.92
3	0.65	6.373	10.98 ± 0.06	324.13	1.50
4	-	5.255	10.98 ± 0.05	324.33	1.42
5	0.05	7.324	11.01 ± 0.04	325.19	1.16
6	0.06	9.151	11.03 ± 0.04	325.88	1.15
7	1.29	9.391	10.87 ± 0.04	321.22	1.19
8	1.38	7.257	10.77 ± 0.04	318.59	1.08
9	1.43	7.278	10.76 ± 0.04	318.16	1.11
10	0.58	8.418	10.85 ± 0.04	320.64	1.20
11	0.27	13.356	10.88 ± 0.03	321.46	0.86
12	-	2.994	10.89 ± 0.13	321.81	3.55
13	-	6.209	10.93 ± 0.08	323.01	2.08
14	1.16	4.109	10.97 ± 0.08	322.96	2.13
15	0.38	5.446	10.93 ± 0.09	322.93	2.53

Integrated age = 321.1 ± 0.4 Ma
Plateau age (steps 10-15) = 322.0 ± 0.8 Ma (1 σ)

Atmospheric contamination (%)	^{39}Ar	^{40}Ar*/^{39}ArK	Apparent age (Ma)	Error (± 1 σ)
Single grain laser analysis. Sample GPK2. Analysis V 947. Steps				
1	17.69	0.60	10.68 ± 0.66	316.03	18.048
2	5.74	1.853	11.12 ± 0.21	327.94	5.67
3	1.20	7.553	10.86 ± 0.06	320.93	1.61
4	1.39	10.684	10.75 ± 0.06	317.87	1.83
5	1.22	6.842	10.82 ± 0.09	319.81	2.49
6	2.19	6.328	10.75 ± 0.08	317.97	2.38
7	0.10	16.784	10.91 ± 0.03	322.35	1.01
8	0.60	9.502	10.81 ± 0.05	319.55	1.53
9	0.16	6.213	10.85 ± 0.07	320.75	2.02
10	0.58	9.898	10.77 ± 0.04	318.55	1.32
11	0.56	14.606	10.81 ± 0.03	319.69	1.02
12	1.13	5.712	10.68 ± 0.09	316.00	2.62
13	0.01	3.424	10.90 ± 0.13	322.07	3.69

Integrated age = 319.1 ± 0.5 Ma
Plateau age (steps 3-13) = 319.8 ± 0.5 Ma (1 σ)

Table 2.- Analytical data for ^{40}Ar/^{39}Ar dates of the Soultz monzogranite.

Tabl. 2.- Données analytiques des datations ^{40}Ar/^{39}Ar du monzogranite de Soultz.

shapes (Table 2; Fig. 2). The GPK2 biotite shows a plateau age of 319.8 ± 0.6 Ma (1σ), representing 97.6% of the released ^{39}Ar. The K2O4 biotite grain was duplicated because of the much more disturbed appearance of the age spectra; both show the characteristic humped shapes that are common for biotites affected by chloritization, explained by a recoil effect of ^{39}Ar from biotite to chlorite layers during irradiation (Lo and Onstott, 1989; Ruffet *et al.*, 1991). However, it has been shown that the high temperature steps can be meaningful if the degree of chloritization is low, which is the case here. The two K2O4 experiments display similar pseudo-plateau ages at 322.8 ± 0.6 Ma (1σ) and 322.0 ± 0.8 Ma (1σ) for respectively 46% and 41% of ^{39}Ar released, which are concordant (at the 2σ level) with the integrated ages of the 321.4 ± 0.04 and 321.1 ± 0.04 Ma. This observation, together with the mean K-Ar age at 321 ± 8 Ma, implies that the ^{39}Ar recoil effect is an internal phenomenon leading to the transfer of ^{39}Ar from different isotopic reservoirs (biotite and chlorite layers) without a net loss of ^{39}Ar. This is corroborated by the shape of the disturbed parts of the two spectra, which show a perfect complementary distribution of the ^{39}Ar-depleted and ^{39}Ar-enriched steps on each side of the apparent highest temperature ages. The high-temperature pseudo-plateau ages obtained on the flat part of the spectra can thus be reasonably considered as geologically meaningful. Moreover, the two distinct ^{40}Ar/^{39}Ar age-spectra shapes obtained for the GPK2 and K2O4 biotite grains are strictly concordant with the mineralogical observations. They reflect the low degree of alteration and chloritization of the deepest part of the wells, which is less affected by geothermal circulation.

The two ^{40}Ar/^{39}Ar ages, obtained on two biotite separates from different depths within the Soultz monzogranite pluton, are undistinguishable at the 2σ level. Moreover, the slight difference between the ages at depths of 3,876 m (319.8 ± 0.6 Ma) and 2,207.5 m (322.4 ± 0.4 Ma) is consistent with a normal top-to-bottom cooling effect and closure of the K-Ar isotopic system during either a general uplift of the geotherm in this area, or a radial cooling of the pluton after its emplacement in a colder environment.

Petrography

The Soultz monzogranite has a porphyritic structure (1 to 8-cm-long K-feldspar megacrysts) set in a granular

matrix (3-4 mm grains) composed of quartz, plagioclase, orthoclase, biotite, amphibole, titanite, allanite and magnetite. Monzonitic texture can be observed. Magmatic layers consisting of up to 60% K-feldspar megacrysts (K134, K136) and of mafic mineral segregations (K91) locally occur. Structural studies using shape-preferred orientation of biotite and K-feldspar megacrysts, show the existence of a bulk subhorizontal magma-flow fabric dominantly oriented to NE. A NW-oriented fabric is superimposed in the upper (Z <1700 m) and lower parts (Z >1950 m) parts of the core, resulting in perpendicular fabrics related to an increase in flattening (Schulmann *et al.*, 1997). Subhorizontal magma fabrics suggest either a laccolithic body (Schulmann *et al.*, 1997), or the roof of a diapir-like intrusion. Subsolidus deformation is shown by weak wavy extinction of quartz and locally brittle feldspar. Post-magmatic fragile fracturing is accompanied by hydrothermal phyllite, sulphide (chalcopyrite, galena) and quartz crystallization, and by pervasive alteration of the wall rock (hematization of feldspars, argillization of plagioclase, alteration of mafic minerals) (Genter and Traineau, 1992; Ledésert *et al.*, 1999). Normative mineral composition (Table 3) indicates low quartz and high feldspar abundances, typical of monzonitic assemblages. The crystallization sequence is summarized in Table 4.

Quartz forms anhedral large crystals (5 to 6 mm), with a slight wavy extinction and characterized by the presence of sets of oriented microcracks with fluid inclusions (Schild *et al.*, 1998; Dezayes *et al.*, 2000).

K-feldspars are anhedral and form millimetre-size perthitic grains associated with quartz and plagioclase in the groundmass. They occur also as euhedral perthitic megacrysts, showing rapakivi texture. K-feldspar megacrysts contain plagioclase, biotite, hornblende, magnetite and titanite inclusions. XRD analyses on megacrysts indicate a high-temperature orthoclase structure. Their composition varies from $Or_{95.9}Ab_{2.9}An_{0.2}Cel_{1.0}$ to $Or_{89.4}Ab_{10.2}An_{0.2}Cel_{0.2}$ (Table 5). In the megacrysts, BaO shows variable contents in the core zone (0.10 to 1.01 wt% BaO) and decreasing contents in the rim zone (0.70 to 0.15 wt% BaO).

	Monzogranite								Enclaves				
	K 75	K 91	K 102	K 119	K 136	K 143	K 155	K 203	K 158	K 130	K 151	K 172	K 138
Quartz	23.6	16.8	22.2	23.2	18.3	21.5	23.2	20.3	5.0	3.8	11.5	11.7	8.8
Orthoclase	25.6	27.2	25.4	18.3	31.0	20.5	19.8	22.7	5.8	16.7	19.4	10.6	37.6
Albite	32.3	35.3	36.5	37.3	35.2	37.8	37.0	37.5	39.6	37.3	34.2	36.2	32.4
Anorthite	8.0	6.9	6.2	8.5	7.0	8.1	9.1	8.6	14.1	10.1	7.8	13.1	6.7
Biotite	7.0	6.9	6.4	11.3	4.6	9.4	5.7	5.6	27.4	16.5	21.5	17.1	11.7
Hornblende	2.0	4.2	1.9	0.4	2.4	1.2	3.4	3.4		12.1		7.6	
Titanite	0.2	0.5	0.2	0.0	0.3	0.2	0.3	0.4	4.5	2.5	2.7	2.9	2.1
Apatite	0.4	0.4	0.4	0.4	0.4	0.5	0.5	0.5	1.4	0.9	1.4	0.8	0.7
Magnetite	0.7	1.3	0.7	0.6	0.7	0.7	0.8	0.8					
Hematite									2.1		1.6		
Total	99.8	99.6	99.8	100.0	99.8	99.9	99.7	99.7	100.0	100.0	100.0	100.0	100.0
Anx	19.9	16.4	14.5	18.5	16.6	17.7	19.7	18.6	20.3	16.2	17.7	25.1	25.5

Table 3.- Normative composition of selected samples from the Soultz monzogranite and associated enclaves calculated using the biotite composition of sample K143.

Tabl. 3.- Composition normative d'une sélection d'échantillons du monzogranite de Soultz et enclaves associées, déterminée en utilisant la composition de la biotite de l'échantillon K143.

Minerais	Sequence of crystallization
Fe-Ti oxides	** relics?
Zircon	*****
Apatite	***** *****
Titanite	** ************** T1 relics?
Magnetite	**************
Biotite	***********
Hornblende	*************
Plagioclase	************ **********
Orthose	************ **********
Quartz	**** **********
Hydrogarnet	******** alteration
Epidote	********
Chlorite	********
Calcite	*****
Oxides	*****
Sericite	****************
Phyllites	***** veins
Quartz	*****
Phyllites	*****
Sulfides	*****

Table 4.- Mineral sequence of crystallization in the Soultz monzogranite.

Tabl. 4.- Course de cristallisation dans le monzogranite de Soultz.

Plagioclase (1-3 mm) is hypidiomorphic (megacrysts) to anhedral (groundmass). Locally, it shows synneusis texture. It is recurrently zoned ($An_{26}Ab_{72}Or_{02}$ in the core to $An_{15}Ab_{84}Or_{01}$ in the border zone; Table 5) and commonly rimmed by albite ($An_{0.5}Ab_{99.1}Or_{0.4}$ to $An_{0.9}Ab_{98.3}Or_{0.8}$).

Biotite forms 1 to 4-mm-large crystals and locally is kinked and/or chloritized. It contains apatite, zircon, titanite and magnetite inclusions. Microprobe analyses give compositions characterized by low Al_2O_3 (14 wt%) and high MgO (13-14 wt%; $0.64<Mg/(Fe_{tot}+Mg)<0.62$) contents coupled with TiO_2 varying from 2.5 to 3.8 wt% (Table 5). This composition does not significantly vary along the well and is comparable to that commonly observed in biotite from high-K calc-alkaline to shoshonitic granites (subalkaline–monzonitic according to Nachit *et al.*, 1985; Stussi and Cuney, 1996). Magnetic separation, heavy liquors and final hand picking carefully purified a biotite aliquot on K102. Biotite purity was tested by XRD and microprobe analyses. The ratio

	Orthoclase							Plagioclase	
	24	2	6	14	20	21	FK-ICP	Plag.1	Plag.22
SiO_2	64.53	63.12	63.26	64.69	64.90	64.36	65.3	64.11	61.72
TiO_2	0.01	0.00	0.00	0.03	0.00	0.00	0.03	0.01	0.01
Al_2O_3	18.86	17.98	18.26	18.40	18.61	18.49	18.00	21.52	22.66
Fe_2O_3	0.18	0.42	0.05	0.15	0.09	0.03	0.17	0.15	0.16
MgO	0.05	0.00	0.00	0.03	0.01	0.03	tr	0.03	0.04
CaO	0.14	0.06	0.04	0.01	0.03	0.03	0.41	0.01	0.01
SrO	0.00	0.00	0.00	0.02	0.00	0.06		3.45	5.11
BaO	0.32	0.44	0.91	0.59	0.20	0.10	0.06	9.62	8.61
Na_2O	2.10	1.48	1.34	0.93	0.91	1.13	3.15	0.41	0.44
K_2O	13.89	14.42	14.64	15.06	15.61	15.05	10.80		
L.O.I.							1.08		
Total	100.70	97.91	98.50	99.91	100.37	99.28	99.10	99.31	98.76
Si	2.969	2.982	2.979	2.993	2.988	2.989	3.019	2.85	2.78
Ti	0.000	0.000	0.000	0.001	0.000	0.000	0.001		
Al	1.023	1.001	1.013	1.003	1.010	1.012	0.981	1.13	1.20
Fe^{3+}	0.006	0.015	0.002	0.005	0.003	0.001	0.006		
Mg	0.003	0.000	0.000	0.002	0.001	0.002	0.000	0.01	0.01
Ca	0.007	0.003	0.002	0.000	0.002	0.002	0.020		
Sr	0.000	0.000	0.000	0.000	0.000	0.002		0.00	0.00
Ba	0.006	0.008	0.017	0.011	0.004	0.002	0.001	0.16	0.25
Na	0.187	0.135	0.122	0.083	0.081	0.102	0.282	0.83	0.75
K	0.816	0.869	0.880	0.889	0.917	0.891	0.639	0.02	0.03
Total	5.017	5.013	5.015	4.988	5.005	5.002	4.945	5.01	5.01
Or	80.3	85.6	86.2	90.4	91.3	89.4	67.8	0.02	0.02
Ab	18.4	13.3	11.9	8.4	8.1	10.2	29.9	0.82	0.73
An	0.7	0.3	0.2	0.0	0.2	0.2	2.1	0.16	0.24
Cel	0.59	0.79	1.67	1.12	0.40	0.20	0.1		

	core				rim
Hornblende	K136.1	K136.7	K136.14	K136.28	K136.39
SiO_2	49.49	45.85	45.92	45.39	44.95
TiO_2	0.46	1.15	1.28	1.38	1.50
Al_2O_3	4.97	6.90	6.93	7.23	7.76
Cr_2O_3	0.01	0.01	0.00	0.01	0.01
Fe_2O_3c	5.42	5.13	3.64	5.13	3.93
FeO	8.97	10.57	11.76	10.32	11.62
MnO	1.00	0.86	0.84	0.72	0.72
MgO	14.07	12.49	12.21	12.66	12.09
NiO	0.03	0.04	0.02	0.04	0.02
CaO	11.50	11.34	11.42	11.32	11.32
Na_2O	1.17	1.53	1.55	1.64	1.72
K_2O	0.47	0.82	0.81	0.86	1.02
Total	97.02	96.18	96.04	96.18	96.28
Si	7.219	6.856	6.923	6.786	6.751
AlIV	0.781	1.141	1.077	1.213	1.249
AlVI	0.072	0.074	0.123	0.061	0.125
Ti	0.050	0.130	0.139	0.155	0.169
Cr	0.001	0.001	0.000	0.001	0.002
Fe^{3+}	0.595	0.577	0.412	0.577	0.445
Fe^{2+}	1.095	1.323	1.477	1.291	1.461
Mn	0.124	0.109	0.114	0.091	0.092
Mg	3.059	2.784	2.733	2.821	2.706
Ni	0.004	0.005	0.002	0.004	0.003
Ca	1.797	1.816	1.833	1.813	1.822
Na(M4)	0.203	0.184	0.167	0.187	0.178
Na (A)	0.129	0.261	0.277	0.289	0.324
K	0.087	0.157	0.153	0.164	0.195
Fe/Fe+Mg	0.263	0.322	0.351	0.314	0.350
Fe^3+/Fe^3+Fe^2	0.352	0.304	0.218	0.309	0.233
% Glauc.	9.95	8.85	7.84	8.96	8.50
% Parg.	22.60	43.04	45.42	46.37	52.87
% Tscher.	15.96	11.68	7.09	11.11	6.09
% Trém.	51.13	35.54	38.66	32.49	31.39
% Cum.	0.35	0.89	0.99	1.06	1.15
Pa/Pa+Tr	30.65	54.77	54.02	58.80	62.75

	Biotite			
	K91	K102	K134	K181
SiO_2	38.09	38.01	37.84	38.05
TiO_2	3.20	3.04	3.61	3.40
Al_2O_3	13.71	13.59	13.82	13.86
Cr_2O_3	0.00	0.01	0.00	0.00
FeOt	16.89	15.74	16.28	16.31
MnO	0.65	0.61	0.48	0.69
MgO	13.62	13.85	13.46	13.59
NiO_2	0.07	0.01	0.03	0.01
CaO	0.00	0.00	0.02	0.00
Na_2O	0.09	0.11	0.14	0.09
K_2O	9.71	9.59	9.68	9.62
F	0.88	0.88	0.88	0.88
H_2O	3.60	3.56	3.58	3.59
O=F	0.37	0.37	0.37	0.37
Total	100.13	98.62	99.43	99.71
Si	5.691	5.733	5.677	5.691
Aliv	2.309	2.267	2.323	2.309
Alvi	0.105	0.149	0.119	0.134
Tivi	0.359	0.345	0.407	0.383
Cr	0.000	0.001	0.000	0.000
Fe^{+3}	0.211	0.199	0.204	0.204
Fe^{2+}	1.899	1.787	1.839	1.836
Mn	0.082	0.078	0.060	0.087
Mg	3.033	3.114	3.010	3.029
Ni	0.008	0.002	0.004	0.001
Ca	0.000	0.000	0.003	0.000
Na	0.025	0.032	0.041	0.025
K	1.851	1.845	1.853	1.835
F	0.416	0.420	0.418	0.416
OH	3.584	3.580	3.582	3.584
Fe/Fe+Mg	0.410	0.389	0.404	0.402
Fe_2O_3c	1.88	1.75	1.81	1.81
FeOc	15.20	14.16	14.65	14.68
Ba		814		
Rb		962		
Sr		6		
ΣTR		34.6		
$(La/Yb)N$		15.7		

Table 5.- Composition of Soultz monzogranite minerals analysed by electron-microprobe (Université Henri Poincaré, Nancy I). Biotite K102: FeO determined by wet chemical analysis; trace elements and REE determined by ICP-MS analyses on separates (C.R.P.G., Nancy-Vandoeuvre). Structural formulas: hornblende: 23 oxygens, 13 cations; magnetite: 32 oxygens, 24 cations (Droop, 1987); ilmenite: 2 cations (Stormer, 1983); hydrogarnet (Rickwood, 1968, after normalization at 5 cations); biotite: 22 oxygens; allanite: 8 cations; titanite: 6 cations.

Tabl. 5.- Composition des minéraux du monzogranite de Soultz déterminée à la microsonde électronique (Services Communs d'analyse, Université Henri Poincaré - Nancy I). Biotite K102 : FeO déterminé par analyse par voie humide ; éléments traces et terres rares déterminés par ICP-MS sur minéraux séparés (C.R.P.G., Nancy-Vandoeuvre). Formules structurales : hornblende : 23 oxygènes, 13 cations ; magnétite : 32 oxygènes, 24 cations (Droop, 1987) ; ilménite : 2 cations (Stormer, 1983) ; hydrogrenat (Rickwood, 1968 ; normalisation à 5 cations) ; biotite : 22 oxygènes ; allanite : 8 cations ; titanite : 6 cations.

$Fe^{3+}/(Fe^{2+}+Fe^{3+}) = 0.11$ (calculated from FeO wet analysis) is significantly lower than that of the whole rock $(Fe^{3+}/(Fe^{2+}+Fe^{3+}) = 0.40$ to 0.60), due to the presence of magnetite in the mineral assemblage. According to Monier (1987), the biotite composition implies the presence of a tetrasilicic mica (MTS) component associated with a relatively high silicic (SiO_2 >37 wt%) and low aluminous composition. ΣREE content is 34.6 ppm and characterized by a high LREE vs. HREE fractionation $[(La/Yb)_N = 15.7]$, possibly slightly modified by the presence of tiny apatite inclusions. The Soultz biotite is characterized by a higher Mg/(Fe+Mg) ratio than most of the biotites from European Variscan calc-alkaline granites (Albuquerque, 1973; Barrière and Cotten, 1979; Neiva, 1981; Pastier and Sabourdy, 1990).

Amphibole forms euhedral (1-4 mm) crystals with recurrent chemical zoning. It contains biotite, zircon, apatite, titanite and magnetite inclusions. The last two minerals are preferably concentrated in the border zone. Amphibole composition is of a magnesian-hornblende type (Leake *et al.*, 1997; Ca >1.5; Na+K <0.65; 0.62 <Mg/(Mg+Fe) <0.75; Si <7.25; Table 5). Microprobe analysis on crystal K136 shows the presence of three zones (Fig. 3a). The rim has strong Mg enrichment, Al^{3+}, Fe^{2+}, Ti^{4+} depletion, and Fe^{3+} increase [Fe^{2+} and Fe^{3+} were calculated from microprobe analyses according to Droop (1987)] compared with the center and core zones. Recurrent zoning of the rim and absence of an actinolitic component in the analysed phase indicated a magmatic rather than subsolidus-re-equilibration origin of this rim zone. A reverse correlation between Ti and Mg, and the increase of Fe^{3+} from core to rim are considered as being associated with a titanite and magnetite climax of crystallization related to increasing oxidation conditions during hornblende crystallization. In some samples, this magmatic zoning is locally disturbed by a patchy actinolitic alteration (K181) characterized by strong but erratic Ti, A-site and Na(M4) depletion (Fig. 3b) associated with an increase of Si and Al^{tot} and a variable Mg/(Mg+Fe) ratio. Anhedral epidote can be associated with the actinolitic subsolidus alteration. Chlorite and calcite are later alteration phases.

Resorbed *Fe-Ti oxides* enclosed in the T1 titanite display exsolution figures of the lamellae-type texture (Haggerty, 1976). In some cases, a later granular aggregate texture (Buddington and Lindsley, 1964) consisting of hematite, ilmenite and ilmeno-rutile or rutile grains, is superimposed on the lamellae texture. The lamellae-textured Fe-Ti oxides display compositional variations that vary from titanian-hematite (2-10 mol.% ilm; MnO = 0-5 wt%) to ferrian and Mn-rich ilmenites (10 wt% <MnO <19 wt%; Table 5). In some ilmenite lamellae, the composition is characterized by a slight TiO_2 excess with respect to the stoichiometric composition of the ilm-hem solid solution (Fig. 4). The high MnO content of the exsolved Mn-ilmenite compared with the Ti-hematite, suggests the crystallization of a pristine Mn-rich ilmeno-

Fe-Ti oxides				
	K155.3.29	K155.3.35	K155.3.36	K155.3.33
SiO_2	0.00	0.00	0.00	0.19
TiO_2	92.01	46.86	16.60	7.51
Al_2O_3	0.00	0.00	0.02	0.00
Cr_2O_3	0.06	0.00	0.03	0.00
$FeOt$	7.99	38.05	71.46	80.62
MnO	0.18	13.39	2.39	0.14
MgO	0.03	0.00	0.00	0.00
CaO	0.24	0.14	0.36	0.63
NiO	0.00	0.08	0.00	0.13
Nb_2O_3	0.36	0.20	0.21	0.06
Total	100.87	98.72	91.08	89.28
Fe_2O_3c	0.00	10.83	66.09	83.09
$FeOc$	7.99	28.32	12.04	5.91
Total	100.87	99.81	97.74	97.66
Si	0.000	0.000	0.000	0.005
Ti	1.812	0.896	0.334	0.152
Al	0.000	0.000	0.001	0.000
Cr	0.001	0.000	0.001	0.000
Fe^{+3}	0.000	0.207	1.330	1.685
Fe^{+2}	0.175	0.603	0.270	0.133
Mn	0.004	0.289	0.054	0.003
Mg	0.001	0.000	0.000	0.000
Ca	0.007	0.004	0.010	0.018
Ni	0.000	0.002	0.000	0.003
Total	2.000	2.000	2.000	2.000
X'ilm	1.00	0.88	0.31	0.14
$MnTiO_3$	0.40	30.43	8.12	0.56
$MgTiO_3$	0.80	0.57	1.56	3.62
$FeTiO_3$	17.51	63.54	40.41	23.02
$Fe_2O_3(R_3)$	0.00	5.46	49.91	72.80
TiO_2	81.30	0.00	0.00	0.00

Magnetite		
	K102.8	K91.85
SiO_2	0.69	0.00
TiO_2	0.00	3.79
Al_2O_3	0.10	0.55
Cr_2O_3	0.16	0.01
$FeOt$	91.52	82.66
MnO	0.00	2.76
MgO	0.35	0.04
CaO	0.10	0.11
NiO		
Nb_2O_3		
Total	92.92	89.96
Fe_2O_3c	67.03	58.30
FeO	31.20	30.20
Total	99.63	95.80
Si	0.212	0.000
Ti	0.000	0.909
Al	0.036	0.207
Cr	0.039	0.003
Fe^{+3}	15.501	13.997
Fe^{+2}	8.019	8.057
Mn	0.000	0.746
Mg	0.160	0.019
Ca	0.033	0.005
Ni		
Total	24.000	24.000
% USP	0.00	11.40
% MGT	99.00	78.19
% Herc	1.00	4.07
% Hém	0.00	6.35

	Titanite		Allanite	
	155.2.1	155.2.10	96.1	96.1
SiO_2	29.65	30.02	30.43	31.67
TiO_2	35.72	35.10	1.66	0.26
Al_2O3	1.27	1.30	11.99	15.42
FeO	2.45	1.86	13.10	13.61
MnO	0.06	0.18	0.75	0.91
MgO			1.30	1.30
CaO	26.28	27.61	10.51	13.00
La_2O_3	0.26	0.04	9.36	4.91
Ce_2O_3	1.35	0.50	9.98	8.27
Pr_2O_3	0.15	0.00	0.45	0.56
Nd_2O_3	0.54	0.09	0.78	1.42
Sm_2O_3	0.03	0.21		
Gd_2O_3	0.02	0.09		
Y_2O_3	0.24	0.35		
Total	98.02	97.35	90.31	91.33
ΣREE	2.35	0.94	20.57	15.16
$Fe2O_3c$			3.82	8.77
$FeOc$			9.67	5.73
Si	1.994	2.008	3.118	3.034
Ti	1.807	1.766	0.128	0.019
Al	0.101	0.102	1.448	1.741
Fe^{+3}	0.138	0.104	0.294	0.632
Fe^{+2}			0.829	0.459
Mn	0.004	0.010	0.065	0.074
Mg			0.199	0.186
Ca	1.894	1.979	1.154	1.334
La	0.006	0.001	0.354	0.173
Ce	0.033	0.012	0.374	0.290
Pr	0.002	0.000	0.008	0.010
Nd	0.013	0.002	0.029	0.049
Sm	0.000	0.000		
Gd	0.000	0.002		
Y	0.008	0.012		
(Ce/La)N	5.2	11.6	0.4	0.6
(Ce/Nd)N	2.6	5.5	9.5	4.3

Hydrogarnet			
	K102.46	K181.66	K169.24
SiO_2	34.48	34.66	34.65
TiO_2	1.30	1.78	2.01
Al_2O_3	6.71	7.65	7.89
Cr_2O_3	0.00	0.00	0.00
FeO	16.68	16.84	17.44
MgO	0.09	0.10	0.05
MnO	0.27	0.00	0.51
CaO	35.39	35.25	35.38
Na_2O	0.00	0.00	0.06
K_2O	0.02	0.00	0.00
H_2Oc	1.31	1.65	2.18
Total	96.25	97.93	100.17
Fe_2O_3c	18.54	17.60	17.54
$FeOc$	0.00	1.00	1.66
Si	2.821	2.779	2.715
H/4	0.179	0.221	0.285
Z	3.000	3.000	3.000
Al	0.647	0.723	0.729
$Fe^{(3+)}$	1.141	1.062	1.034
Ti	0.080	0.107	0.119
Cr	0.000	0.000	0.000
Y	1.868	1.893	1.881
$Fe^{(2+)}$	0.000	0.067	0.109
Mg	0.011	0.012	0.006
Mn	0.019	0.000	0.034
Ca	3.102	3.028	2.970
X	3.132	3.107	3.119
Andradite (+Ti)	65.7	62.3	61.8
Pyrope	0.4	0.4	0.2
Spessartine	0.7	0.0	1.2
Hydrogrossular	6.3	7.7	9.9
Grossular	26.9	29.6	26.8

Tabl. 5 (suite)

Fig. 3.- (a) Element variation along a profile across a zoned hornblende crystal from sample K136. (b) Actinolitic alteration displayed by Na(M4) vs. A-site variations in hornblende from sample K181 (open circles), compared with unaltered hornblende K136 (black squares). Abbreviations: md: magmatic differentiation; alt: subsolidus actinolitic alteration; c.p.f.u: number of cations per formula unit; pt: point of analysis; data represent the mean composition of 4 to 25 single analyses from homogeneous zones obtained across a 1-mm-long profile consisting of 350 points; width of zones 0.01-0.07 mm.
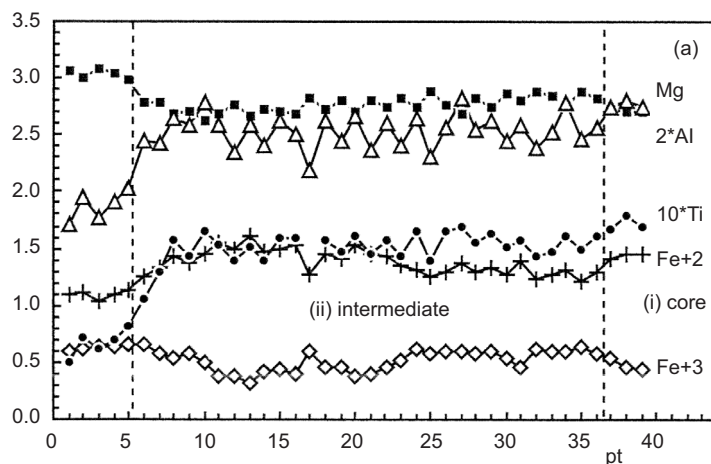
Fig. 3.- (a) Variation des éléments dans un cristal de hornblende zonée (échantillon K136). (b) Mise en évidence de l'altération actinolitique par les variations de Na(M4) versus site-A. Abrévations : alt : altération actinolitique subsolidus ; c.p.f.u. : nombre de cations par formule unitaire ; pt : numéro du point d'analyse ; chaque donnée représente la composition moyenne de 4 à 25 analyses ponctuelles de zones homogènes traversées le long d'un profil de 1 mm de long et comportant 350 analyses ; largeur des zones : 0,01 à 0,07 mm.
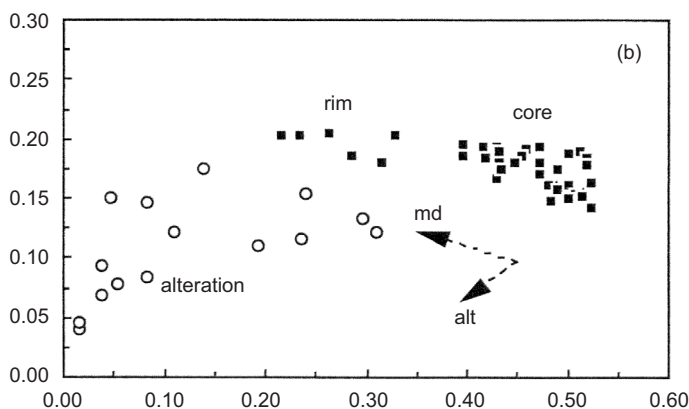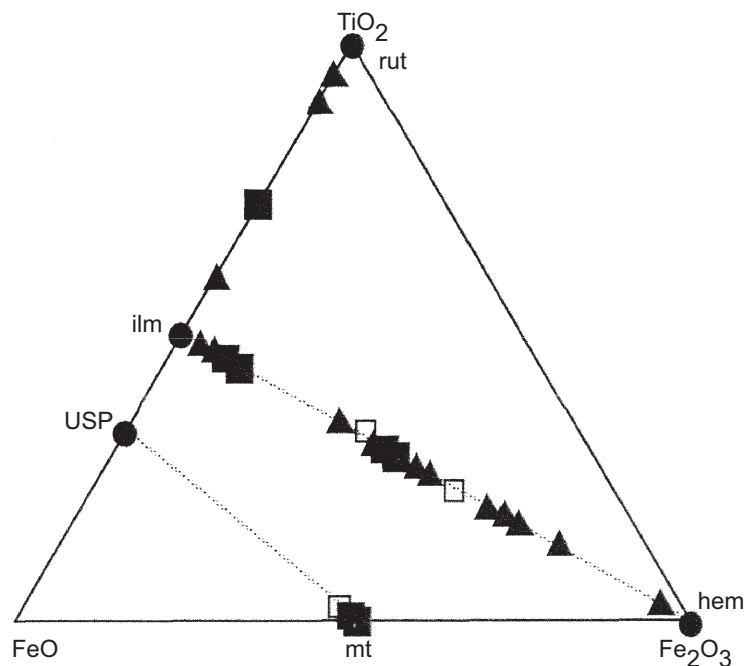
Fig. 4.- Composition of the Fe-Ti oxides (molar proportions). USP: ulvöspinel; mt: magnetite; ilm: ilmenite; hem: hematite; rut: rutile. Black squares: sample K143; black triangles: sample K102; open squares: sample K155.

Fig. 4.- Composition des oxydes ferro-titanés (proportions molaires). USP : ulvöspinel ; mt : magnétite ; ilm : ilménite ; hem : hématite ; rut : rutile. Carrés noirs : échantillon K143 ; triangles noirs : échantillon K102 ; carrés blancs : échantillon K135.
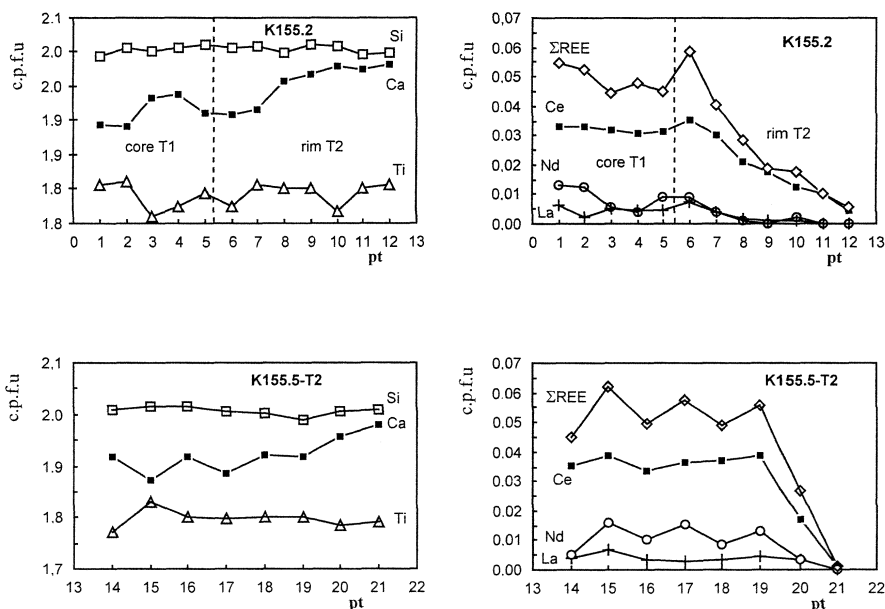

Fig. 5.- Variation of Si, Ca, Ti, La, Ce, Nd and ΣREE in zoned titanites. K155 2: titanite composed of T1 core and T2 border zone (distance between analyses: core: 0.05 mm; rim: 0.025 mm). K155-5: T2 titanite unhosting T1 core (distance between analyses 0.02 mm). c.p.f.u: number of cations per formula unit; pt: point of analysis.

Fig. 5.- Variations de Si, Ca, Ti, La, Ce, Nd et somme des terres rares dans les sphènes zonés. K155-2 : sphène à coeur T1 et bordure T2 (distance entre analyses : coeur : 0,05 mm ; bordure : 0,025 mm). K155-5 : sphène T2 dépourvu de coeur T1 (distance entre analyses : 0,02 mm). c.p.f.u. : nombre de cations par formule unitaire.

hematite. Ilmenite is observed only as resorbed and exsolved crystals in the core of titanite T1, suggesting that this oxide represents either early crystallizing phases or, more probably, relicts of the source materials. Magnetite forms euhedral, isolated or aggregated (together with titanite ± hornblende) crystals and occurs as inclusions in hornblende and biotite. Its composition is very homogeneous, and close to that of stoichiometric magnetite (USP <1 wt%; Fig. 4; Table 5). Hematitic subsolidus oxidation develops as rims and along subsolidus cracks.

Titanite forms euhedral to subhedral crystals (0.5-1.5 mm), commonly associated with magnetite and hornblende crystals without reactional rims. Fe-Ti oxides, calcite and rutile are usual subsolidus alteration products. Titanite displays a complex compositional recurrent zoning, in some crystals combined with sector zoning (fir-tree and/or complex zoning) comparable to that described by Paterson and Stephens (1992) from Caledonian granites. REE show two main compositional zoning types (Fig. 5; Table 5):

- *(i) Core zone (titanite T1)* that shows recurrent chemical zoning and resorbtional textures. It contains exsolved and resorbed ilmenite inclusions;

- *(ii) Rim zone (titanite T2)*, the recurrent chemical zoning of which is marked by a decreasing REE and Ti content reversal correlated to the Ca content (sample K155.2-T1/T2 in Fig. 5), and by irregular variations of the Ce/La, Ce/Pr and Ce/Nd ratios. In some cases, La is undetected in the outermost rim. The boundary between T1 and T2 is irregular but sharp, and results from resorbtion processes of T1 before T2 crystallization. Many of the observed titanite crystals do not contain T1 titanite. The variation of their Ca, Ti, Si, and REE contents is slightly less marked than that in the T2 border of T1-hosting titanite (sample K155.5-T2 in Fig. 5). T1 and T2 (core zone) titanites are marked by comparable ranges of ΣREE contents and $(La/Yb)_N$ ratios (Table 5; Figs. 5 and 6).

Apatite occurs as (i) small crystals included in biotite, hornblende and magnetite, and as (ii) euhedral crystals (0.2-0.5 mm long) associated with the quartz-feldspar groundmass. Its fluorine content varies from 3.8 to 4.8 wt%. *Allanite* is scarce and altered. BSE images

display a complex chemical zoning that consists of snow-ball-like or curved plume-like textures in the core zone, presumably resulting from rapid crystallization, rimmed by less REE-enriched and recurrently zoned allanite. Sector-like zoning also occurs. In a single crystal, the ΣREE content varies from 15 to 20 wt% oxides (mean 19.4 wt%). LREE are strongly enriched, with higher REE fractionation compared with titanite (Table 5; Fig. 6). *Zircon* represents a subordinate accessory phase compared with titanite. *Epidote* is an alteration product associated with hornblende and plagioclase, or of possibly primary origin as crystals growing epitaxically on allanite. *Hydrogarnet* (Table 5) is observed as an early alteration product of biotite associated with chloritization; it occurs as lenses parallel to the cleavage.

The Soultz monzogranite contains round microgranular mafic enclaves that vary in thickness from 2 to 25 cm (Traineau *et al.*, 1991). They usually form a fine- (<1 mm) to medium-grained texture, locally with a planar structure. The mineral assemblage consists of plagioclase, orthoclase, hornblende and biotite (the only ferro-magnesian mineral in K158). Early existence of a preexisting clinopyroxene is suggested by the presence of quartz symplectites in the core of some hornblende crystals. Some 0.2 to 3-cm-long phenocrysts (or xenocrysts?) of the following minerals are observed, possibly inherited from the monzogranite host: plagioclase, K feldspar, quartz, biotite, hornblende hosting clinopyroxene relicts (sample K130-3126a; 1749.05 m). Accessory minerals are titanite, magnetite and needle-shaped apatite. The composition of the mineral assemblage varies from monzogabbrodiorite (K158) through quartz-monzodiorite and quartz-monzonite to quartz-syenite; tonalite varieties are also observed. The core of one enclave (K174-4191; 2038.64 m) contains a hornfels-type rock characterized by a granoblastic and planar structure composed of polygonal plagioclase, poikiloblastic hornblende and accessory titanite, magnetite and apatite; this is surrounded by a mesocratic, hypidiomorphic, porphyritic and K-feldspar-rich rock of similar composition to the quartz-monzonite enclaves.
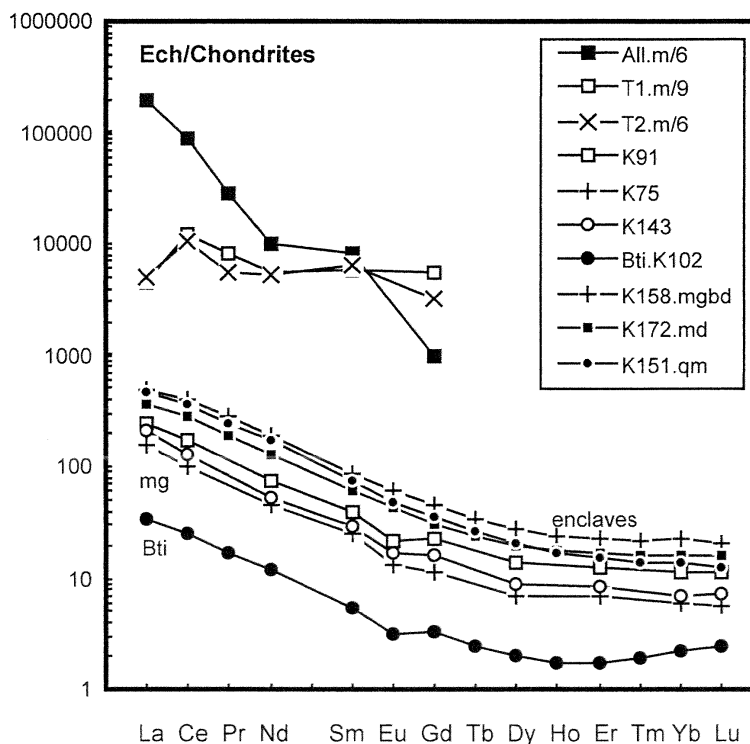

Fig. 6.- REE fractionation patterns (normalized after Evensen *et al.*, 1978) of titanite, allanite, biotite, monzogranite and enclaves of the Soultz intrusion. All: allanite; T1, T2: titanite 1 and titanite 2; bti: biotite (K102); mg : monzogranite.

Fig. 6.- Spectres de terres rares (normalisées aux chondrites selon Evensen et al.*, 1978) du sphène, de l'allanite, de la biotite, du monzogranite et des enclaves de l'intrusion de Soultz. Abréviations : cf. légende anglaise.*

Whole-rock chemistry

Bulk composition of the Soultz monzogranite (Table 6) is characterized by silica content varying from 67.0 to 69.0 wt%, and relatively high Na_2O (~4 wt%), CaO (~2 wt%), K_2O (~4.5 wt%) contents. K_2O (>5.5 wt%) and $Fe_2O_3+MgO+TiO_2$ (>5.8 wt%) are significantly higher in samples marked by K-feldspar (K134, K136) and mafic mineral segregations (K91). The TiO_2 content (0.40-0.50 wt%) indicates a high titanium activity in the magma, yielding the crystallization of titanite and Ti-rich biotite. In spite of the abundance of Mg-rich minerals (biotite, hornblende), the X_{Mg} of the whole rock is relatively low (0.45) due to the crystallization of magnetite controlled by high f_{O2}. Whole-rock composition shows metaluminous characteristics (molar ratio $Al_2O_3/(CaO+Na_2O+K_2O)$ <1.0) due to the presence of hornblende and titanite. Altered members (K109, K178) are marked by leaching of Ca and Na due to phyllic alteration of plagioclase and chloritization of biotite and hornblende.

According to Debon and Le Fort (1988), the Soultz monzogranite shows an intermediate composition between quartz-monzonite and granite (Fig. 7).

Trace element contents such as Ba (625–998 ppm) and Sr (480-634 ppm) are high, although lower than in the HiBaSr granitoids (Tarney and Jones, 1994). Maximum values of Ba and Sr are observed in the K-feldspar and biotite layering (Table 6). Th (24 to 37 ppm), U (6.2 to 14.1 ppm) and ΣREE (193 to 260 ppm) contents are high. The $La_{(N)}$ (150 to 250 times that of the chondrite-normalized content) and $[La/Yb]_N$ values (19 to 31) show the contribution of titanite and allanite (Fig. 6). ΣREE is depleted in the most altered sample (K178), indicating a loss of the REE during alteration of titanite.

The Soultz monzogranite shows a high-K calc-alkaline magma composition (Peccerillo and Taylor, 1976; Mg-K calc-alkaline composition according to Cocherie *et al.*, 1994). In spite of a slightly

N°	K 75	K 91	K 96	K 102	K 109	K 119	K 134	K 136	K 143	K 155	K 169	K 178	K 181	K 203	K130	K138	K151	K158	K172
				Monzogranite													Enclaves		
Z in m	1423	1533	1560	1606	1642	1692	1776	1797	1850	1930	2011	2072	2089	2202	1748	1814	1915	1955	2023
SiO_2	68.67	65.00	68.62	69.06	68.27	68.15	65.56	67.81	67.65	68.43	67.09	70.81	67.25	67.70	56.67	60.73	58.15	52.46	58.18
TiO_2	0.44	0.68	0.44	0.44	0.48	0.48	0.54	0.40	0.52	0.51	0.55	0.40	0.56	0.52	1.10	0.83	1.09	1.85	1.23
Al_2O_3	14.36	14.92	14.85	14.41	14.67	14.67	15.41	15.31	14.88	14.48	15.01	13.08	15.00	14.98	16.90	16.76	17.05	17.80	16.00
Fe_2O_3t	2.83	4.37	2.77	2.79	2.67	3.04	3.40	2.56	3.16	3.16	3.37	2.25	3.33	3.12	6.96	4.62	5.81	8.35	6.43
MnO	0.06	0.10	0.06	0.06	0.04	0.05	0.08	0.05	0.07	0.06	0.07	0.08	0.07	0.06	0.22	0.12	0.15	0.20	0.19
MgO	1.18	1.46	1.11	1.10	0.81	1.56	1.54	0.93	1.41	1.20	1.33	0.48	1.36	1.20	3.09	1.32	2.53	3.36	3.02
CaO	2.12	2.32	2.02	1.77	1.20	2.00	1.76	2.00	2.12	2.62	2.65	2.07	2.49	2.54	4.27	2.29	3.11	4.98	4.50
Na_2O	3.52	3.84	4.08	4.00	0.53	4.08	4.08	3.87	4.14	4.04	4.15	2.54	4.16	4.12	4.79	3.75	4.00	4.72	4.45
K_2O	4.91	5.16	4.65	4.84	7.05	4.15	5.49	5.62	4.34	3.84	4.08	4.12	4.19	4.33	4.68	7.18	5.29	3.63	3.44
P_2O_5	0.17	0.20	0.17	0.17	0.22	0.20	0.19	0.17	0.22	0.22	0.24	0.19	0.24	0.22	0.44	0.30	0.60	0.62	0.35
P.F.	1.44	1.53	0.90	0.96	3.76	1.30	1.60	0.85	1.09	1.05	1.14	3.66	1.01	0.82	1.21	1.41	1.44	1.22	1.23
Total	99.70	99.58	99.67	99.60	99.70	99.68	99.65	99.57	99.60	99.61	99.68	99.68	99.66	99.61	100.33	99.31	99.22	99.19	99.02
Fe_2O_3c	1.59	2.69	1.21	1.23	1.75	1.24	1.57	1.08	1.34	1.27	1.44	0.68	1.34	1.31	n.d.	n.d.	n.d.	n.d.	n.d.
FeO	1.12	1.51	1.40	1.40	0.83	1.62	1.65	1.33	1.64	1.70	1.74	1.41	1.79	1.63	n.d.	n.d.	n.d.	n.d.	n.d.
Xmg	0.45	0.40	0.44	0.44	0.38	0.50	0.47	0.42	0.47	0.43	0.44	0.30	0.45	0.43	0.47	0.36	0.46	0.44	0.48
Ba	691	998	813	883	626	732	1237	1414	922	776	848	958	908	981					
Cr	19	31	21	15	16	17	26	24	25	23	21	15	19	18					
Nb	6	30	8	18	19	10	21	15	20	22	19	5	20	15					
Ni	15	21	15	10	19	12	18	11	13	18	15	9	16	15					
Rb	221	241	201	204	357	164	232	219	183	167	169	178	176	172		384	315	301	198
Sc	5.4	9.3	5.5	4.9	4.5	5.5	6.5	5.0	5.8	6.4	6.6	4.5	6.4	6.1					
Sr	364	429	516	483	135	441	509	557	525	520	599	190	634	606	599				
Th	32.7	55.3	34.3	37.1	34.9	34.7	44.5	32.2	30.2	24.0	31.7	27.5	30.2	35.0	26.9	27.9	28.7	18.6	18.7
U	10.4	12.0	8.6	14.1	12.4	11.7	9.4	9.1	6.2	6.6	11.5	6.3	9.7	7.6	5.0	6.7	6.3	4.9	4.6
V	43	68	42	38	40	41	52	39	47	48	52	28	51	46					
Y	14.4	28.3	18.1	18.0	11.9	20.1	20.9	16.6	18.2	18.4	20.7	13.0	21.5	23.0	33	37	28	41	28
Zn	38	63	43	43	29	43	67	36	49	46	47	32	47	43					
Zr	168	304	164	172	186	185	198	160	190	194	193	156	202	208					
La	57.32	90.98	53.64	68.43	54.17	61.11	68.32	59.77	78.70	55.11	58.34	52.56	58.04	61.09	109.20	92.00	112.20	119.90	87.20
Ce	97.74	163.88	96.47	119.48	101.43	109.97	127.20	101.39	123.88	103.24	116.90	94.07	114.37	115.65	241.60	201.40	226.60	258.20	180.20
Pr															31.91	22.00	23.75	17.20	18.21
Nd	31.76	53.91	33.46	36.77	33.43	37.91	40.84	33.60	37.90	35.91	42.37	31.95	42.67	40.24	113.30	79.60	82.85	88.91	60.02
Sm	5.64	9.07	6.12	6.81	5.94	6.74	7.38	6.61	6.65	6.26	7.13	5.27	7.64	7.26	15.75	12.04	11.69	13.14	9.23
Eu	1.17	1.90	1.30	1.35	1.22	1.44	1.63	1.36	1.43	1.33	1.55	1.13	1.60	1.52	3.16	2.40	2.70	3.56	2.54
Gd	3.46	7.02	4.44	4.99	4.04	4.69	5.30	4.14	4.89	4.35	5.29	3.32	6.14	5.16	7.50	7.95	7.28	9.22	6.28
Tb															1.38	1.16	0.97	1.27	0.90
Dy	2.69	5.33	3.33	3.40	2.42	3.48	3.72	3.17	3.34	3.25	3.88	2.47	3.93	3.54	6.88	6.77	5.16	7.13	5.05
Ho															1.30	1.26	0.95	1.38	0.98
Er	1.69	3.10	1.88	2.20	1.59	2.21	2.29	2.00	2.06	1.90	2.22	1.39	2.47	2.21	3.62	3.62	2.58	3.84	2.73
Tm															0.57	0.51	0.36	0.56	0.40
Yb	1.48	2.76	1.70	1.76	1.29	1.84	1.96	1.60	1.71	1.74	2.00	1.23	2.00	1.80	3.69	3.31	2.29	3.70	2.66
Lu	0.22	0.43	0.25	0.30	0.21	0.28	0.31	0.25	0.27	0.28	0.28	0.18	0.32	0.31	0.52	0.46	0.31	0.53	0.40
□REE	203.2	338.4	202.6	245.5	205.7	229.7	259.0	213.9	260.8	213.4	240.0	193.6	239.2	238.8	540.38	434.48	479.69	528.54	376.80
(La/Yb)N	26.17	22.28	21.32	26.27	28.38	22.44	23.55	25.24	31.10	21.40	19.71	28.88	19.61	22.93	20.0	18.8	33.1	21.9	22.1
(La/Sm)N	6.40	6.31	5.52	6.32	5.74	5.71	5.83	5.69	7.45	5.54	5.15	6.28	4.78	5.30	4.4	4.8	6.0	5.7	5.9
(Gd/Yb)N	1.89	2.06	2.12	2.30	2.54	2.07	2.19	2.10	2.32	2.03	2.14	2.19	2.49	2.32	1.6	1.9	2.6	2.0	1.9
Eu/(Eu)N	0.75	0.70	0.73	0.68	0.72	0.74	0.76	0.74	0.73	0.74	0.74	0.77	0.69	0.72	0.78	0.71	0.83	0.94	0.97

Table 6.- Bulk composition of Soultz monzogranite and associated enclaves. Monzogranite analyses: ICP-EC and ICP-MS, C.R.P.G. Nancy-Vandoeuvre, France. Enclave analyses: ICP-ES, B.R.G.M. Orléans, France. K158: monzogabbrodiorite; K172 and K130: monzodiorites; K151: quartz-monzonite; K138: quartz-syenite.

Tabl. 6.- Composition chimique (roche totale) du monzogranite de Soultz et des enclaves associées. Monzogranites : ICP-EC et ICP-MS, C.R.P.G. Nancy-Vandoeuvre, France. Enclaves: ICP-ES, B.R.G.M. Orléans, France. K172 et K130 : monzodiorites ; K151 : monzonite quartzifère ; K138 : syénite quartzifère.

higher plagioclase abundance, this magma composition is close to that observed in several shoshonitic plutons from the Vosges (Natzwiller, Senones and Ballons massifs), northern Black Forest (Baden-Baden) and northeastern Bohemia (Meissen Massif) (Pagel and Leterrier, 1980; Wenzel et al., 1997; Altherr et al., 2000; Fig. 7). It is more potassic than the Champ-du-Feu calc-alkaline suite (Deschamps, 1995) and contrasts with the calc-alkaline (Waldhambach, Windstein) and peraluminous (Edenkoben, Burrweiler) granitoid intrusions along the Rhine Graben Escarpment (Bassahak and Gagny, 1987; Reischmann and Anthes, 1996). Compared with the Odenwald

intrusive complex, its composition differs strongly from the calc-alkaline Neunkirch granitoids (O.UII in Fig. 7) (Barth, 1972), but it shares some major-element characteristics with the Heidelberg and Tromm younger granites (Odenwald-Unit III; H and T in Fig. 7; Altherr et al., 1999). With regard to the trace element signature, the last two, however, are less Th, U, Rb, Y, P, and REE enriched than the Soultz, Senones and Natzwiller monzogranites (Altherr et al., 2000). These differences could be related with the composition of their respective source rocks.

The composition of the enclaves varies from monzogabbrodiorite through quartz-

monzodiorite to quartz-monzonite and quartz-syenite; they are enriched in Th, Y and REE (<540 ppm; $19<(La/Yb)_N<33$) compared with the host monzogranite (Table 6; Fig. 6). Their shoshonitic magma composition is comparable to that of several Variscan monzonitic suites such as the southern Vosges, the NE Bohemian Meissen massif (Fig. 7), and the western French Massif Central (Pagel and Leterrier, 1980; Wenzel et al., 1997; Rolin et al., 1999; Cuney et al., 2001). These enclaves have comparable major-element compositions to those observed in Unit III from the Odenwald (Altherr et al., 1999), though they are more Th, Y and REE enriched.

The whole-rock composition of the Soultz monzogranite has been processed with a multivariate statistical method in order to highlight zonal variations along the drill core. The principal component analysis (PCA) chosen for that purpose used 24 elements (major + trace elements) and 15 samples distributed along the drill-hole, but excluded all altered samples. The logs of chemical data and of PCA factors show two zones (Fig. 8):

- *A lower zone* (Z >1800 m) is characterized by plagioclase and mafic-minerals (Fe+Mg+Ti) enrichment. In this zone, the high Ba, Sr V, P contents and Sr/Th and K/Ba ratios regularly decrease upwards;

- *An upper zone* (Z <1800 m) is enriched in orthoclase, quartz, and depleted in mafic minerals (Fe+Mg+Ti) and plagioclase. This zone shows low Sr, Ba, Zr, V, P, and ΣREE, and high Th, U contents. Contrary to the lower zone, the Ba, Sr, V, P element content and mineral abundances decrease (Sr, Ba) or increase (K/Ba, Th, U) irregularly upwards. Plagioclase composition is slightly more albitic than in the lower zone.

The vertical mineralogical and chemical variations within the monzogranite intrusion can be interpreted as resulting from intraplutonic mineral segregation during ascent and/or emplacement of the magma in a relatively static chamber. According to mass-balance calculation, a best fit of the segregation simulation is obtained considering the mean composition SZ9 of nine analysed samples (excluding altered and cumulate samples) as a starting magma, rather than segregation operating in the lowermost lower sample of the drilled intrusion. According to Langmuir (1989), the lowermost zone can be considered as a cumulate zone with regard to the uppermost zone.

Discussion

Crystallization conditions

The absence of clinopyroxene in the mineral assemblage (megacrysts, relicts in hornblende) is consistent with a more-evolved Soultz monzogranite composition compared with other Variscan monzogranites in which this mineral is observed (i.e., in the Ballons monzogranite:
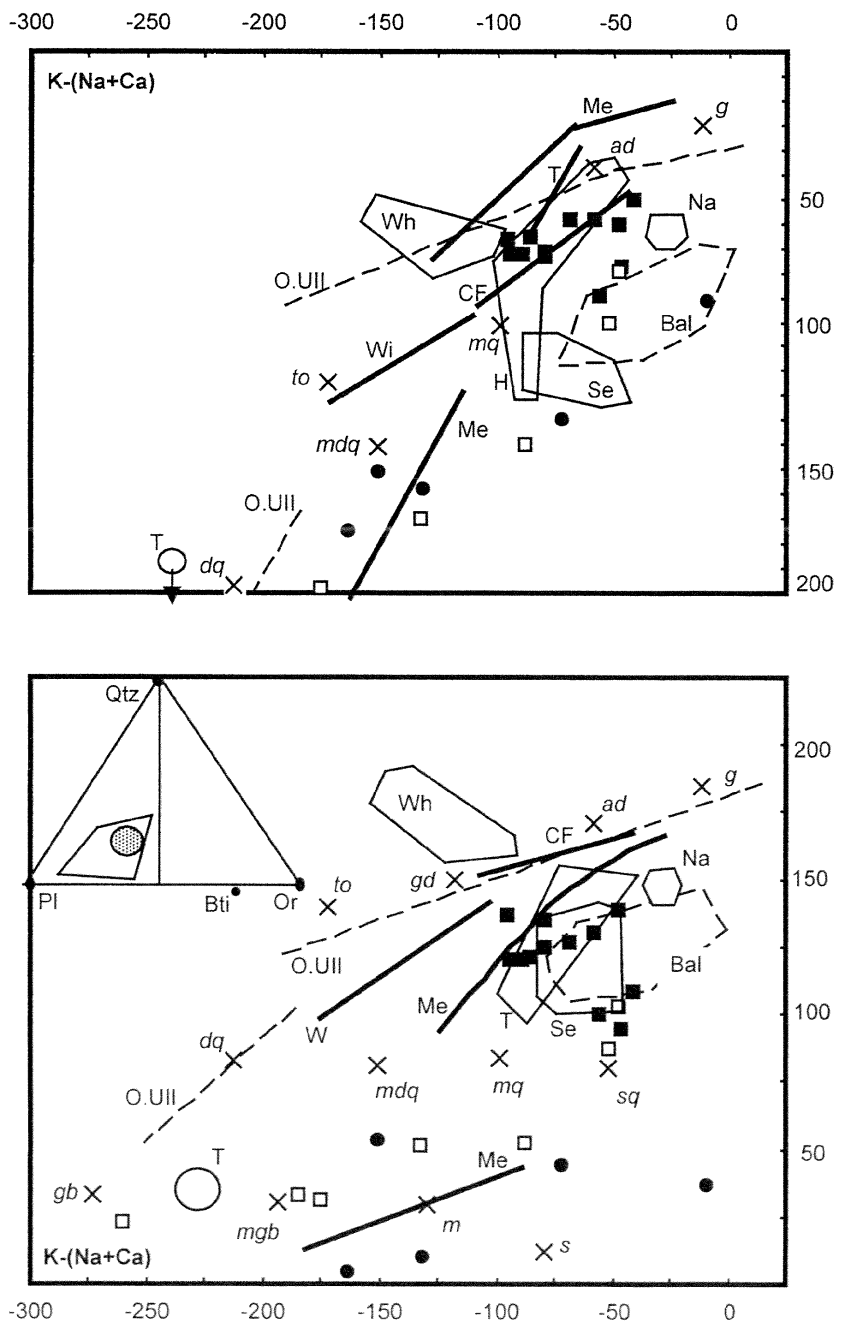
Fig. 7.- Chemical characterization of Soultz monzogranite (black squares) and associated enclaves (filled circles) in the diagram for plutonic-rock classification (Debon and Le Fort, 1988); comparison with granitoids from adjacent areas.
Northern Vosges: Wi: Windstein; Se: Senones; Na: Natzwiller; CF: Champ-du-Feu; Southern Vosges: Bal: Ballons monzogranite; open squares: Ballons monzogabbro to quartz monzonite intrusions; Odenwald: O.UII: Odenwald-Unit II diorite and granitoid; H: Heidelberg granite; T: Tromm granite (Odenwald-Unit III); Me: monzonitic Meissen suite (N Bohemian massif); Wh: Waldhambach (West Rhine river escarpment).
to: tonalite; gd: granodiorite; ad: adamellite; g: granite; mdq: quartz-monzodiorite; mq: quartz-monzonite; sq: quartz-syenite; gb: gabbro; mgb: monzogabbro; s: syenite; dq: quartz-diorite; m: monzonite. Qtz: quartz; Pl: plagioclase; Or: orthoclase; bti: biotite.

Fig. 7.- Caractérisation chimique du monzogranite de Soultz (carrés noirs) et enclaves associées (disques noirs) dans le diagramme de classification des roches plutoniques selon Debon et Le Fort (1988). Comparaison avec les granitoïdes des régions adjacentes. Vosges du Nord : Wi : Windstein ; Se : Senones ; Na : Natzwiller ; CF : Champ-du-Feu ; Vosges du Sud : Bal : monzogranite des Ballons ; carrés blancs : monzogabbro à monzonites quartzifères des Ballons ; Odenwald : O.UII : diorites et granitoïdes de l'Odenwald-unité II ; H et T : granites de Heidelberg et de Tromm (Odenwald-unité III) ; Me : suite monzonitique de Meissen (N du massif de Bohême) ; Wh : Waldhambach (talus rhénan occidental).
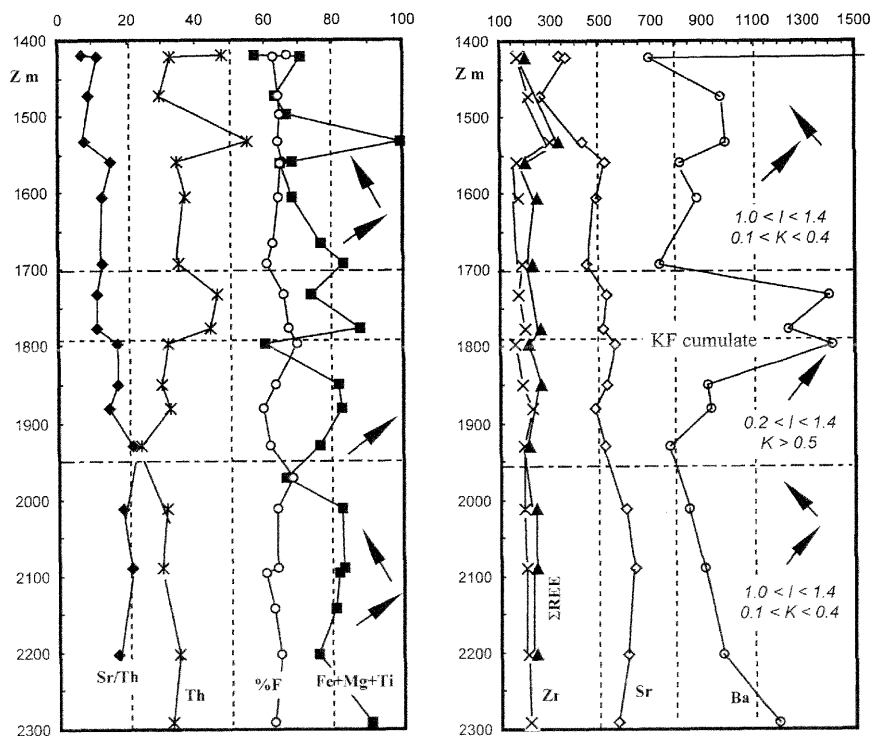
Fig. 8.- Element-variation logs in the Soultz monzogranite along the EPS-1 drill-hole showing the existence of two chemical zones. Structural data from Schulmann *et al.* (1997). Arrows: magmatic lineation; I: deformation intensity; K: symmetry of structure.

Fig. 8.- Mise en évidence de deux zones chimiques par les logs des variations élémentaires dans le sondage EPS-1 du monzogranite de Soultz. Données structurales selon Schulmann et al. *(1997). Flèches : linéations magmatiques ; I : intensité de la déformation ; K : symétrie de la structure.*

64 wt%<SiO_2<68 wt%, relictual CPX in hornblende and presence of An_{40-45} plagioclase; Pagel and Leterrier, 1980). In addition, the absence of this mineral is also controlled by a higher water content and lower temperature in the magma than those required for pyroxene stability (Naney, 1983).

The crystallization of biotite in equilibrium with K-feldspar prior to the main stage of hornblende-crystallization is consistent with the experimental data of Naney (1983) in granodioritic systems at conditions in excess of 800°C and at 200 Mpa, for magmas containing less than 4 wt% H_2O. The high rate of crystallization of late hornblende with respect to biotite indicates an increase in the H_2O content (>4 wt%) with decreasing temperature in the magma (<780 °C at 200 MPa).

Habitus and chemical zoning of hornblende in the monzogranite indicate that this mineral is a liquidus phase. The absence of reactional contacts between hornblende and coexisting minerals suggests that hornblende is stable at the

magmatic conditions and does not result from clinopyroxene alteration. It coexists with magnetite and titanite as early as the crystallization of K feldspar in which it is included. The presence of magnetite in equilibrium with a magnesian-rich hornblende, suggests a rightward displacement of the equilibria TiFeparg (FeTi component of hornblende) + Qz + O_2 <—> Mt + Plag + Sph or Fetrem + ilm + O_2 <—> Mt + plag + Sph (Wones, 1989). Using the Al^{tot}-in-hornblende geobarometer of Schmidt (1992), the calculated crystallization pressure of hornblende varies from 2.4 to 3.7 kb in respectively the intermediate and core zones (3.3 to 4.9 kb using the Al^{IV}-in-hornblende geobarometer of Blundy and Holland (1990)). In the rims, the pressure drops down to 1.0<Pkb<1.5 kb (1.1<Pkb<1.9 kb using the Al^{IV} content). As shown by Holland and Blundy (1994) and Anderson and Smith (1995), the Al content of hornblende depends also on the temperature and plagioclase composition. Assuming that a mean crystallization pressure of 3.5 kb and a plagioclase composition X_{Ab} = 0.70, the crystallization temperature of hornblende from the inter-

mediate and core zones is in the range of 750 to 785°C (Holland and Blundy, 1994). A temperature of about 663 and 715°C is obtained for the rim for respectively [P = 3.5 kb; X_{Ab} = 0.70] and [P = 1.5 kb; XAb = 0.80]. Since the nature of the surrounding rocks is unknown, the P,T conditions of the intrusion depth and of magma consolidation cannot be further constrained by local geological features. The depth of intrusion (4 to 10 km) is in the range of that of many of the western MGCR granitoids (Flöttmann and Oncken, 1992; Henk, 1995; Oncken, 1997). It is also in the same range of intrusion depth as that of the Early Carboniferous granitoids intruding Late Devonian to Early Carboniferous, weakly deformed, and low to very low-grade metasedimentary rocks from other European Variscan areas (Cuney, 1978; Rossy, 1978; Pagel and Leterrier, 1980; Wickert and Eisbacher, 1988; Altherr *et al.*, 2000).

The temperature calculated with the Al^{tot}-in-hornblende thermometer is lower than that obtained with biotite thermometry (Patino-Douce, 1993). The latter yields a crystallization temperature in the range of 820-890°C at 3.5 kb. This temperature is consistent with a crystallization temperature of 800°C for biotite (Naney, 1983) and with the high crystallization temperature of Ti- and Mg-rich biotite (Patino-Douce, 1993). The difference between the Al-in-hornblende and biotite thermometers can be due to the early crystallization of biotite with respect to the main stage of hornblende crystallization.

Titanite does not show reactional figures with other mafic minerals. Its euhedral habit and textural relationships with biotite, magnetite and hornblende suggest that it was a liquidus phase at a temperature close to 740°C and a pressure below 4 kb (Spear, 1981). The presence of titanite together with Ti-rich biotite and magnetite indicates a Ti- and REE-rich and oxidized magma. The presence of resorbed T1 titanite cores suggests either disequilibrium conditions during the early crystallization of titanite, or, more probably, refractory phases derived from the source materials. The recurrent REE zoning of T2 titanite reflects the variation of the REE behavior during crystallization in the magma (Mittlefieldt and Miller, 1983; Michael, 1984; Sawka, 1988). Together with the presence of zoned plagioclase, K-feldspar and hornblende, it suggests that

the monzogranitic magma evolved by processes involving fractional crystallization influenced by magma heterogeneities, element diffusion, magma contamination, and by pressure and temperature.

Since ilmenite is a relictual phase as shown by its textural features, the ilmenite-magnetite pairs cannot be used for estimating the crystallization temperature and the f_{O2} (Buddington and Lindsley, 1964; Carmichael, 1967; Czamanske and Mihalik, 1972; Spencer and Lindsley, 1981). According to the experimental studies of Spear (1981), titanite crystallizes in equilibrium with magnetite at f_{O2} close to the HM buffer rather than to the QFM buffer. The low Fe^{3+}/Fe^{2+} ratio (0.114) of biotite associated with magnetite and titanite, suggests oxidizing conditions close to or above those of the NNO buffer at the biotite crystallization stage (Fe^{3+}-Fe^{2+}-Mg^{2+} diagram not shown). The difference between the Fe^{3+}/Fe^{2+} ratios of chlorite-free biotite (0.114) and whole rock (0.74), probably results from buffering by mineral equilibria, i.e. the increasing oxidizing conditions associated with Fe consumption by magnetite crystallization cause an increase of Mg^{2+} activity in the magma and in the crystallization of a Mg-rich hornblende (Czamanske and Wones, 1973; Czamanske et al., 1981; Wones, 1989). Assuming that the hornblende core crystallizes together with biotite close to the NNO buffer, and taking into account the increase in the Fe^{3+}/Fe^{2+} ratio in hornblende from the core to the rim zone, $logf_{O2}$ will increase with decreasing temperature and pressure by two units during hornblende crystallization (-13.8 $<logf_{O2}<$-15.2 for the NNO buffer at P = 3.5 kb; -11.6$<logf_{O2}<$-13.2 for the HM buffer at P = 1.5 kb; Fig. 9).

Based on the calculated pressure and temperature of hornblende crystallization, a two-stage history is proposed for crystallization of the Soultz monzogranite:

- (i) An early stage of crystallization occurred in a deep-seated magma chamber (3 to 4 kb [9-12 km]; 750°C<T°C<790°C). This chamber probably was an intermediate one, because at this depth and considering a geothermal gradient in the range of 50°C/km, the expected temperature is not higher than 650°C. This regional geothermal gradient can be related to crustal thickening consistent with a collisional to

postcollisional stage and/or to a regional abnormally hot mantle;

- (ii) A late stage of crystallization occurred after adiabatic ascent of the magma. This stage is characterized by the consolidation of the quartz-feldspar matrix at the solidus after crystallization of the hornblende rim zone. The pressure was about 1.5 kb (4.5 to 5.0 km depth) for 665°C<T°C<715°C. The consolidation stage was followed by progressive exhumation of the basement associated with fluid circulation, up to the presently observed level of occurrence of the intrusion.

No obvious relationships are seen between the observed vertical chemical variations (present study) and the magma fabrics with depth (Schulmann et al., 1997; Fig. 8). This discrepancy, which contrasts with other case studies done on boreholes (Gagny and Cuney, 1997; Cuney et al., 1999), suggests that the magma fabrics do not result from successive supply of magma during emplacement of the pluton, as also shown by the absence of contacts between the structural or chemical zones. It argues rather for a heterogeneous magma flow related to differential strain with depth (Schulmann et al., 1997) during the late stage of magma emplacement prior to magma consolidation, and most probably after development of the chemical polarity in a presumably more static environment. The K-feldspar cumulates might represent laminae related to local higher strain, resulting in K-feldspar segregation associated with a "filter-press process" of interstitial magma.

Cooling ages. Uplift

The mean ages of 325 ± 6 Ma (Rb/Sr) (Rummel, 1991) and 321 ± 8 Ma (K/Ar), obtained by two independent geochronological methods, indicate similar cooling ages of the Soultz monzogranite. Considering analytical errors, these ages are not significantly different from the 331 ± 9 Ma emplacement age obtained through U/Pb on zircon dating (Alexandrov et al., 2001). A more precise estimate of the cooling age has been obtained by $^{40}Ar/^{39}Ar$ dating. Analyses of biotite grains from two samples located at 2207 and 3876 m gave ages of 322 ± 1 Ma and 320 ± 1 Ma respectively, showing a significant age difference of only 2 ± 1 Ma. It can be used for esti-
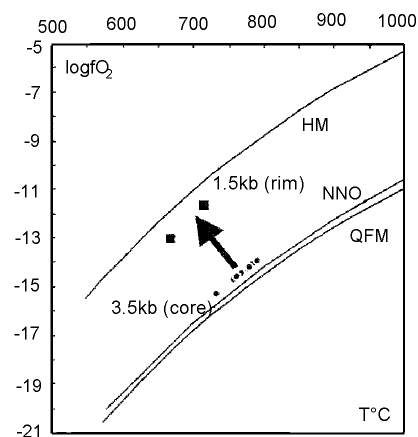
Fig. 9.- Logf$_{O2}$ versus temperature (T°C) variation estimated from hornblende composition (K136). Symbols: squares at 1.5 kb (border zone of hornblende); filled circles at 3.5 kb (core of hornblende); solid lines hematite-magnetite (HM), Ni-NiO (NNO) and quartz-fayalite-magnetite (QFM) buffers at 1 kb using data from Wones (1989).

Fig. 9.- Variation de logf$_{O2}$ avec la température (T°C) dans la hornblende de l'échantillon K136. Symboles : carrés à 1,5 kb (bordure des cristaux) ; disques noirs à 3,5 kb (coeur de l'amphibole) ; traits continus : tampons hématite-magnétite (HM), Ni-NiO (NNO) et quartz-fayalite-magnétite (QFM) à 1 kb selon Wones (1989).

mating an uplift rate of about 0.5 ± 0.15 mm.yr^{-1} considering an uncertainty of the depth of the sample (cutting). This uplift rate agrees with that given by Henk (1995) for the Late Variscan exhumation rate of the Rheno-Hercynian zone, and for the western Mid-German Crystalline Rise. The equilibrium temperature of the surrounding rocks, estimated at 360°C, is in the range of the K-Ar isotopic closure temperature for biotite (250-450°C; Armstrong et al., 1966; Villa and Puxeddu, 1994), suggesting that the post-magmatic uplift of the Soultz monzogranite took place at about 320 Ma.

Origin

An origin of the high-K calc-alkaline and shoshonitic granitoids through crustal partial melting of metamorphic greywacke, granulite and amphibolite, has been suggested by Sheppard (1986) and Pin and Duthou (1990), or of metaigneous rocks of appropriate composition (Roberts and Clemens, 1993). A purely crustal origin through dehydration melting of metasedimentary rock is proposed for the origin of the northern
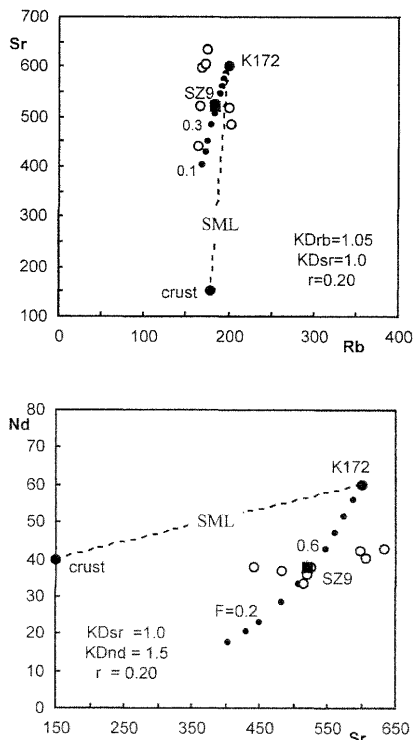
Fig. 10.- Assimilation fractional crystallization (AFC) modelling using Sr-Rb and Nd-Sr pairs, for deciphering the origin of the Soultz monzogranite assuming a crustal protolith and a mafic mantle- or lower-crust-derived component represented by enclave K172.
SML: simple mixing line. SZ9: mean composition of the monzogranite (n = 9, omitting cumulate and altered samples). Open circles: Sr-Rb and Nd-Sr correlation among the samples, transversal on the model, show mineral segregation within the monzogranite.

Fig. 10.- Simulation du processus d'assimilation-cristallisation fractionnée (ACF) d'après les couples Rb-Sr et Nd-Sr en vue de tester l'origine du monzogranite de Soultz. On considère un processus impliquant un protolithe crustal et un constituant mantello-dérivé représenté par l'enclave K172. SML : droite de mélange simple. SZ9 : composition moyenne du monzogranite (n = 9, cumulats et échantillons altérés non pris en compte). Disques blancs : corrélations Sr-Rb et Nd-Sr dans les échantillons, transverses au modèle et traduisant les effets des ségrégations de minéraux dans le monzogranite étudié.

Vosges shoshonitic monzogranite by Altherr *et al.* (2000). However, a purely metasedimentary origin of the monzogranite suggests two remarks:

- Metagreywackes, used as starting material for experimental melting studies, are characterized mostly by a peraluminous composition (Conrad *et al.*, 1988; Vielzeuf and Montel, 1994 ; Patino Douce and Beard, 1995). Their melting yields a peraluminous melt whose composition is inconsistent with the metaluminous composition of high-K calc-alkaline to shoshonitic monzogranite;

- The presence of mafic to intermediate phases as intrusions and/or enclaves, associated with monzogranite intrusions with which they present obvious converging chemical features, suggests the existence of probable genetical relationships and of chemical and mechanical interactions among the coexisting phases. Thus, some minor mantle-derived contribution in the monzogranite origin cannot be excluded.

According to Rummel (1991), the $^{87/86}Sr$ initial ratio (0.7058) of the Soultz monzogranite indicates a crustal origin involving the contribution of a mantle-derived component. This value is slightly lower than that obtained for the southern Vosges Ballons monzogranite ($^{87/86}Sr_{(330)}$ = 0.7069; Schaltegger *et al.*, 1996) and is in the range of those obtained for the northern Vosges younger granites (0.70457<Sr_i<0,70598; Altherr *et al.*, 2000). All these monzogranites have a major-element composition close to that of Soultz monzogranite (cf. Fig. 7) and are marked by negative εNd values (1.9<εNd<3.4) that are interpreted as resulting from a mainly crustal origin of the magmas, possibly involving a small mantle contribution (Langer *et al.*, 1995; Altherr *et al.*, 2000).

The presence of monzogabbrodiorite to quartz-monzonite and quartz-syenite enclaves in the Soultz monzogranite, shows the development of a mafic to intermediate magmatism coeval with the monzogranite magma. The converging petrological features observed at Soultz among the monzogranite and its associated enclaves (i.e. magma nature, high K, Th, U, and REE enrichment, similarity in REE patterns; Fig. 6), suggest a genetical relationship between these phases as already investigated by several studies on granitoids and their enclaves [Didier and Barbarin (1991) and attached references]. These relationships can be attributed to (i) mechanical and chemical interaction between a crustal magma and a mantle-derived magma, to (ii) a fractional crystallization process in the mafic source, or to (iii) assimilation - fractional-crystallization (AFC). Assuming a mantle contribution in the origin of the Soultz monzogranite as shown by Rummel (1991), the less differentiated monzodi-

orite and monzogabbrodiorite enclaves may represent a mantle derived component. Although no isotope data are available on these enclaves to constrain their origin, the less differentiated phases may represent mantle-derived magmas, as also considered in many basic-acid plutonic complexes (Holden *et al.*,1987; Dias and Leterrier, 1994; Cuney *et al.*, 1999). Their K, LIL, and HFS-element enrichment would result either from the melting of an enriched upper mantle or from mantle-derived magmas that suffered some crustal contamination (Foley *et al.*, 1987; Bingen *et al.*, 1993; Wenzel *et al.*, 1997; Debon and Lemmet, 1999). Such mantle-derived magmas may suffer fractional crystallization and/or intrude the lower continental crust, in which they induce anatexis yielding crustal magmas with which they may present mechanical and chemical interactions.

Mass-balance calculation and simulation of Rb, Sr, Ba trace-element fractionation, show that the origin of the monzodiorite is inconsistent with a model of fractional crystallization from monzogabbrodiorite. The latter represents either a distinct mantle-derived magma involving the partial melting of a biotite-rich peridotite, or, more probably, a biotite cumulative phase resulting through segregation of plagioclase, pyoxene and amphibole from a monzodiorite magma. Thus, the monzogabbrodiorite cannot be the pristine mantle-derived component and the K172 monzodiorite will be considered as the most probable mantle-derived component involved in the origin of the monzonitic suite and monzogranite. At this stage, we cannot assess whether the monzodiorite derives directly from the partial melting of an enriched mantle source, or from a mantle derived component already involved in the lower crust at an earlier stage of the regional geotectonic evolution, and possibly contaminated by crustal magmas. The following models in the origin of the monzogranite will be discussed hereafter:

(i) The monzogranite (represented by its the mean composition SZ9) may result from the mixing of K172 monzodiorite (42%) and a felsic magma (58%) with a composition close to the minimum melt and containing about 1.5% of biotite. This mixing model is likely, but improbable because it involves an important mantle-derived component, contrary to

PERIOD	EPOCH	AGE	MAGMA COMPOSITION		
			Peraluminous	High-K Calc-alkaline Shoshonitic	Calc-alkaline
PERMIAN		290			
CARBONI-FEROUS	Stephan.	303			
Silesian	Westphalian	311		321 ± 8 § Soultz 319.0 ± 0.5 # Soultz 322.4 ± 0.4 # Soultz	320 ± 10 § Andlau Gr
	Namurian	323 327		325 ± 6 ** Soultz 325 ± 4 § Senones	
Dinantian	Visean		326 ± 6 Meissen Haupt-granit	328 ± 4 # Senones 329.8 ± 1.0 # Meissen.Leuben hb1 329.4 ± 1.0 # Meissen.Leuben hb2 329.1 ± 1.4 # Meissen.Mz.hb1 330.4 ± 1.4 # Meissen.Mz.hb2 330.5 ± 5.3 * Kagenfels 330.7 ± 4.6 # Kagenfels bti 330 ± 4 § Natzwiller Gr. Bti 331 ± 9 * Soultz	326 ± 5 § Neuntelstein D. Hb 328 ± 4 § Andlau Gr. Bti 328 ± 4 § Champ-du-Feu Gd. Hb 329 ± 4 § Waldersbach Gr. Bti 329 ± 4 # Waldersbach Gr. Bti 329-326 ± 4 § OW-UII. Hb, bti 330.5 ± 3.0 # Champ-du-Feu Gd. Hb 330 § Champ-du-Feu.Diorite.bti 330 ± 10 § Waldersbach G. 331 ± 3 # Neuntelstein D. hb 331 ± 12 # Hohwald Gd-D. hb 332 ± 11 # Holwald.Gr.Bti 336-332 ± 4 § OW-UIII. Hb, bti 333 ± 6.9 * Burrweiler 333.1 ± 4.4 * Waldhambach 333.7 ± 3.7 * Windstein 333.9 ± 1.0 # Windstein bti 335 ± 4 § Waldersbach Gr. Bti 335 § OW-UII. Gr/hb
				338 ± 2 # Natzwiller bti	338 ± 4 § OW-UII. Gd. Bti
			335 ± 9 * Edenkoben 339 ± 34 *** Edenkoben	340.4 ± 1.2 # Natzwiller bti	
		342		341.6 ± 0.6 # Kagenfels bti	342 § OW-UII.granite
	Tournaisian				344 § OW-UII. Granodiorite hb 346-333 § OW-UII. Gd. Hb, bt
		354			
DEVONIAN					362 ± 7 # Frankenstein gabbro OW-UI 362 ± 9 * Frankenstein gabbro OW-UI 369 * Albersweiler orthogneiss
Late		370			
Middle		391			
Lower		417			

Table 7.- Summary of ages obtained for plutonic rocks from Soultz, western Rhine river escarpment, northern Vosges, and Odenwald; distribution according to magma composition. Data sources: Hellman *et al.*, 1982; Kirsch *et al.*, 1988; Rummel, 1991; Boutin *et al.*, 1995; Edel and Weber, 1995; Hess *et al.*, 1995; Reischmann and Anthes, 1996; Wenzel *et al.*, 1997; Altherr *et al.*, 1999, 2000; this study.
Abbreviations: OW-UI, OW-UII, OW-UIII: Odenwald units I, II and III; Gr: granite; Gd: granodiorite; D: diorite; Mz: monzonite; hb: hornblende; bt: biotite. Dating symbols: *: U/Pb; **: Rb/Sr; ***: Sm/Nd; #: $^{40}Ar/^{39}Ar$; §: K/Ar.

Tabl. 7.- Datations absolues obtenues sur les roches plutoniques de Soultz, du talus rhénan occidental, des Vosges du Nord et de l'Odenwald. Répartition selon les types de magmatisme. Abréviations : OW-UI, OW-UII, OW-UIII : Odenwald Unités I, II et III ; autres abréviations et sources des données : cf. légende anglaise.

that suggested by the $\epsilon Nd_{(330)}$ of the Ballons massif (Langer *et al.*, 1995) of comparable composition to the Soultz monzogranite. It also implies a felsic protolith enriched in Th (37 ppm) and REE (167 ppm) with regard to the mean crustal composition. In addition, it is poorly constrained by the variation of the X_{Mg} number from monzodiorite (0.48) to monzogranite (0.44-0.47).

(ii) An alternative hypothesis suggests that the Soultz monzogranite derived from a parental K172 monzodiorite magma through simple fractional crystallization. This model implies the segregation of 52% of cumulate consisting of pyroxene, amphibole, biotite and plagioclase. This model also shows some discrepancies with the fractionation rates estimated from Rb and Sr, and with the compatible behaviour patterns of the REE. In addition, a stronger decrease of X_{Mg} in the monzogranite would be expected instead of that observed. Thus, the simple fractional crystallization model can be rejected.

(iii) AFC models using Sr-Rb and Nd-Sr pairs (no $^{87}Sr/^{86}Sr$ and Sm/Nd available data for the mafic component, nor Sm/Nd data for the monzogranite) yield a more likely process for the origin of the monzogranite. As shown in Fig. 10, the best fit is obtained for r = 0.20 and F = 0.50, similar to the F = 0.48 value obtained by major-element mass-balance calculation. The r value is lower than the upper limit of r = 0.3 recommended by Taylor (1980) for assimilation. Although it has to be constrained by complementary Sm/Nd

isotope data, this AFC model is close to that invoked for the origin of several high-K calc-alkaline to shoshonitic granitoid complexes of similar composition from the European Variscan (Ballons massif: Pagel and Leterrier, 1980; Corsica: Cocherie *et al.*, 1994; North Bohemian Meissen massif: Wenzel *et al.*, 1997; overburden Charroux-Civray massif: Cuney *et al.*, 1999, 2001; Hercynian Alps plutonic complexes: Debon and Lemmet, 1999).

Regional correlations

The Soultz monzogranite differs in composition from the western MGCR calc-alkaline (Waldhambach, Windstein, Kaiserbachtal, Odenwald) and peraluminous (Edenkoben, Burrweiller) intrusions in that it is of a high-K calc-alkaline-magma type. Its emplacement, accompanied by coeval and less differentiated shoshonitic magmas only observed as enclaves, has no homologue in the Rhine Graben escarpment intrusions. It represents the only high-K calc-alkaline monzogranite intrusion presently known to occur between the northern Vosges calc-alkaline (Champ-du-Feu) and shoshonitic (Natzwiller, Kagenfels, Senones) intrusions to the west, and the high-K calc-alkaline to shoshonitic granites of the Odenwald-Unit III to the northeast. Farther east, in the northern Bohemian Massif, it can be compared to the monzonitic phases of the post-collisional Meissen plutonic complex (329.1 ± 1.4 to 330.6 ± 1.8 Ma: $^{40}Ar/^{39}Ar$ dating on hornblende; Wenzel *et al.*, 1997).

At Soultz, cooling ages of 325 ± 6 Ma (Rb/Sr on whole rock; Rummel, 1991) and 322 ± 1 to 320 ± 1 Ma ($^{40}Ar/^{39}Ar$ ages; this study; Fig. 2) are not significantly distinct from the U/Pb-on-zircon emplacement age of 331 ± 9 Ma (Alexandrov *et al.*, 2001). These ages are the youngest observed among the Western MGCR plutonic bodies, indicating that magmatic activity lasted from 342 to 320 Ma along the MGCR (Table 7; Hellman *et al.*, 1982; Boutin *et al.*, 1995; Hess *et al.,* 1995; Reischmann and Anthes, 1996; Altherr *et al.*, 2000). The Soultz monzogranite postdates the calc-alkaline Windstein granodiorite and the shoshonitic Senones and Natzwiller intrusions. Compared to the Neunkirch calc-alkaline plutonic complex from the Odenwald Unit II (Krohe, 1991), no plastic deformation has been observed

in the Soultz monzogranite. Thus, the Rb/Sr and $^{40}Ar/^{39}Ar$ dates obtained on the Soultz intrusion being close to its emplacement age, it postdates the strike-shear and associated extension tectonics of the D3 phase affecting the wall rocks and controlling the emplacement of diorite and granodiorite (K-Ar dating on hornblende at 342 Ma; Hellman *et al.*, 1982) of the Odenwald Unit II (Krohe, 1991). It is coeval with, or possibly postdates, the 336-326 Ma old granitoids of the Odenwald Unit III (K-Ar dating on hornblende and biotite; Hellman *et al.*, 1982; Altherr *et al.*, 1999) associated with extensional tectonics of the D4 phase (Krohe, 1991; Willner *et al.*, 1991).

Two principal interpretations are generally invoked for the emplacement of the MGCR plutonic rocks:

- The MGCR is considered as a Late Devonian magmatic arc, related to the south-directed subduction of the Rheic ocean, followed in the Early Carboniferous by oblique continental collision between Laurentia/Baltica and the northern edge of Gondwana (Franke 1989a, b; Willner *et al.*, 1991; Edel and Weber, 1995; Franke *et al.*, 1995). According to Altherr *et al.* (1999), the 362 ± 2 Ma old gabbrodiorite (Kirsch *et al.*, 1988) was emplaced in an arc-type setting during the Late Devonian; it was followed by subduction- to syn-collision-related diorite and granitoid intrusions during the Early Carboniferous, in the Odenwald and in the northern Vosges. Faure *et al.* (1997), ascribe the origin of the northern Vosges and northern Massif Central and Vendée diorites, to the Late Devonian southward subduction of the Rheic ocean under the northern edge of the extensional Gondwana margin. However, the northern Vosges diorite and associated granite and granodiorite, dated at 340-330 Ma, are as a whole younger than the diorite and associated tonalite and granodiorite from the Massif Central and Vendée, dated at 373 to 350 Ma (Rolin *et al.*, 1999; Cuney *et al.*, 1999, 2001) and thus probably correspond to younger collisional events. The presence within the MGCR of calc-alkaline, high-K calc-alkaline, and peraluminous phases emplaced from 345 to 325 Ma in a single geotectonic environment, suggests an origin through crustal anatexis, possibly induced by mantle-derived intrusions represented by gabbrodiorite and/or

diorite. In addition, although the initial geometric relationships between the MGCR and the central Vosges are not known, Deschamps (1995) argues that it is difficult to reconcile the existence of an oceanic subduction-related magmatism coeval with the development of major peraluminous magmatism in the Central Vosges. Thus, the emplacement of the various magmas types in a single geotectonic space and time span argues for a mainly crustal-magma activity related to Carboniferous collisional- to post-collisional tectonics. This can be compared with the Early Carboniferous magma activity characterizing the internal parts of the Western European Variscan (Rolin *et al.*, 1999; Cuney *et al.*, 1999, 2001; Colchen et Rolin, 2001).

- The MGCR is a crustal rootless unit floating on underthrust Rheno-Hercynian and Saxo-Thuringian zones (Onken, 1997) that formed from 335 to 305 Ma in relation with continental subduction. It would contain relics of an early Carboniferous magmatic arc, and no magmatic input would be expected after the initial continental collision at 335 Ma (Onken, 1997) because of the loss of the asthenospheric source. This interpretation implies that the MGCR intrusions belong to a preexisting magmatic arc, formed before the initial amalgamating tectonics. However, the presence of the Soultz intrusion shows that magma activity still occurred during this time.

The Soultz monzogranite thus is interpreted as being the youngest plutonic manifestation of the Western MGCR related with the continent-continent evolution of this zone. Coeval with the Senones and Natzwiller shoshonitic intrusions, with which it present close compositional similarities, it is an ultimate manifestation of a magmatic stage characterized by the production, from 342 to 325 Ma (Table 7) and in a single geotectonic context, of magma types whose origin involves various parts of the continental and subcontinental lithosphere.

Conclusions

A granitoid intrusion below Soultz-sous-Forêts, selected for the experimental HDR heat exchanger, has been studied by means of samples from a 1000-m-long section of the EPS-1 drill-hole. The

intrusion is located beneath Mesozoic and Cenozoic sedimentary rocks in the Rhine Graben valley, north-northwest of Strasbourg. It consists of a metaluminous Ca-, Mg-, K-rich monzogranite marked by high lithophile (Th, U, REE) element contents and presents a high-K calc-alkaline magma nature. The monzogranite was emplaced around 331 Ma, followed by cooling period down to 325–320 Ma. It has a mainly crustal origin ($^{87/86}$Sr initial ratio = 0.7058) involving a mantle-derived component. The latter is assumed to be represented by less differentiated monzodiorite enclaves (closest composition to a mantle-derived component) in the monzogranite. An assimilation-fractional crystallization (AFC) model is the most likely process for the origin of this monzogranite as also shown by the recurrent chemical zoning of K-feldspar (Ba), hornblende, plagioclase, titanite (REE) and allanite (REE), and the development of partial-resorbtion processes affecting some phases. Crystallization history is distinguished by two main stages:

(i) *A deep-seated stage* characterized by crystallization temperature and pressure in the range of 755-790°C and 3.5 kb respectively, corresponding to a depth of about 11 to 12 km.

(ii) *A final consolidation stage* occurring at a higher crustal level, characterized by a lower crystallization temperature and pressure (T°C = 665-715°C; P = 1.5 kb) corresponding to a depth of about 4.5 to 5.5 km. This depth of emplacement, which cannot be further refined, is in the range of those observed for several granitoid intrusions from the MGCR and from various segments of the Western European Variscan (e.g. southern Vosges, northeast French Massif Central).

The Soultz monzogranite represents a newly observed high-K calc-alkaline manifestation within the MGCR, which is mainly marked by the presence of sub-coeval to coeval calc-alkaline to high-K calc-alkaline granitoids, and subordinate shoshonitic and peraluminous granitoids (northern Vosges and Black Forest; Odenwald; western Rhine Graben escarpment). It presents some converging features with the final intrusions from the Odenwald Unit III and especially with the latest northern Vosges shoshonitic intrusions. The origin of the various magma types, which originated in a single geotectonic environment during a time-span of about 20 Ma, involves distinct magma sources in the continental and subcontinental lithosphere during this stage of geotectonic evolution of the MGCR. The production of these magmas was most probably related to collisional to post-collisional tectonics that developed during Visean to Namurian times.

Acknowledgements

References

Albuquerque D.C.A.R. (1973) - Geochemistry of biotites from granitic rocks, Northern Portugal. *Geochim. Cosmochim. Acta,* **37**, 1779-1802.

Alexandrov A., Royer J.J., Deloule E. (2001) - 331 ± 9 Ma emplacement age of the Soultz monzogranite (Rhine Graben basement) by U/Pb ion-probe zircon dating of samples from 5 km depth. *C.R. Acad. Sci. Paris,* **332**, 747-754.

Altherr R., Henes-Kleiber U., Hegner E., Satir M., Langer C. (1999) - Plutonism in the Variscan Odenwald (Germany): from subduction to collision. *Int. Journ. Earth Sciences*, **88**, 422-443.

Altherr R., Holl A., Hegner E., Langer C., Kreuzer H. (2000) - High-potassium calc-alkaline I-type plutonism in the European Variscides: northern Vosges (France) and northern Black Forest (Germany). *Lithos,* **50**, 51-73.

Anderson J.L., Smith D.R. (1995) - The effects of temperature and f$_{O2}$ on the Al-in hornblende barometer. *Am. Mineral.,* **80**, 549-559.

Armstrong R.L., Jäger E., Eberhardt P. (1966) - A comparison of K-Ar and Rb/Sr ages on Alpine biotites. *Earth. Planet. Sci. Lett.,* **1**, 13-19.

Barrière M., Cotten J. (1979) - Biotite and associated minerals as markers of magmatic fractionation and deuteric equilibration in granites. *Contrib. Mineral. Petrol.,* **70**, 183-192.

Barth H. (1972) - Petrologische Untersuchungen im Felsberg-Zug (Bergsträsser Odenwald). *Abh. hess. L-Amt. Bodenforsch.,* **66**, 85 p.

Bassahak J., Gagny C. (1987) - La granodiorite de Windstein, Bas-Rhin, France : un témoin de la cohorte des « granites rouges » vosgiens. Congrès Soc. Savantes Lyon, S. Sciences, 33-43.

Bingen B., Demaiffe D., Hertogen J., Weis D., Michot J. (1993) - K-rich calc-alkaline augen gneisses of Grenvillian Age in SW Norway: mingling of mantle-drived and crustal components. *J. Geol.,* **101,** 763-778.

Blundy J.D., Holland T.J.B. (1990) - Calcic amphibole equilibria and a new amphibole-plagioclase geothermometer. *Contrib. Mineral. Petrol.,* **104**, 208-224.

Boutin R., Montigny R., Thuyzat R. (1995) - Chronologie K-Ar et ^{39}Ar-^{40}Ar du métamorphisme et du magmatisme des Vosges. Comparaison avec les massifs varisques voisins. *Géologie de la France,* **1**, 3-25.

Bresee J.C. (Ed.) (1992) - Geothermal energy in Europe: the Soultz Hot Dry Rock Project. Gordon and Breach, Newark, N.J., 309 p.

Buddington A.F., Lindsley D.H. (1964) - Iron-titanium oxide minerals and synthetic equivalents. *J. Petrol.,* **5**, 310-357.

Carmichael I.S.E (1967) - The iron-titanium oxides of salic volcanic rocks and their associated ferromagnesian silicates. *Contrib. Mineral. Petrol.,* **14,** 36-64.

Clauser C. (1989) - Conductive and convective heat flow components in the Rheingraben and implications for the deep permeability distribution, *in* Hydrogeological Regimes and Their Subsurface Thermal Effects, A.E. Beck, G. Garven, L. Stegnar (eds) , *Geophys. Monogr. Ser.,* **47**, A.G.U. Washington D.C., 59-64.

Cocherie A., Rossi P., Fouillac A.M., Vidal P. (1994) - Crust and mantle contributions to granite genesis. An example from the Variscan batholith of Corsica, France, studied by trace-element and Nd-Sr-O-isotope systematics. *Chem. Geol.,* **115**, 173-211.

Colchen M., Rolin P. (2001) - La chaîne hercynienne en Vendée. *Géologie de la France,* **1-2**, 53-86.

Conrad W.K., Nicholls I.A., Wall V.J. (1988) - Water-saturated and -undersaturated melting of metaluminous and peraluminous crustal compositions at 10 kb: evidence for the origin of silicic magmas in the Taupo Volcanic zone, New Zealand, and other occurrences. *J. Petrol.,* **29**, 765-803.

Cuney M. (1978) - Geologic environment, mineralogy and fluid inclusions of the Bois-Noirs - Limouzat uranium veins, Forez, France. *Econ. Geol.,* **73**, 1567-1610.

Cuney M., Brouand M., Stussi J.M., Gagny C. (1999) - Le massif de Charroux-Civray : un exemple caractéristique des premières manifestations plutoniques de la chaîne hercynienne. *In:* Etude du massif de Charroux-Civray, Actes Journées scientifiques CNRS/ANDRA, Poitiers 13-14 October 1997, EDP Sciences (Ed.), 91944, Les Ulis, France, 63-104.

Cuney M., Brouand M., Stussi J.M., Virlogeux D. (2001) - Le complexe plutonique de Charroux-Civray (Vienne) : témoin du magmatisme infra-carbonifère dans le segment occidental de la chaîne varisque européenne. *Géologie de la France,* **1-2**, 143-166.

Czamanske G.K., Mihalik P. (1972) - Oxidation during magmatic differentiation, Finnmarka Complex, Oslo Area, Norway: part 1, the opaque oxides. *J. Petrol.,* **13**, 493-509.

Czamanske G.K., Wones D.R. (1973) - Oxidation during magmatic differentiation, Finnmarka Complex, Oslo Area, Norway: part 2, the mafic silicates. *J. Petrol.,* **14**, 349-380.

Czamanske G.K, Ishihara S., Atkin S.A. (1981) - Chemistry of rock-forming minerals of the Cretaceous-Paleocene batholith in southwestern Japan and implications for magma genesis. *J. Geophys. Research,* **86**, 10431-10469.

Debon F., Le Fort P. (1988) - A cationic classification of common plutonic rocks and their magmatic associations: principles, method, applications. *Bull. Minéral.,* **111**, 493-510.

Debon F., Lemmet M. (1999) - Evolution of Mg/Fe ratios in Late Variscan plutonic rocks from the external crystalline massifs of the Alps (France, Italy, Switzerland). *J. Petrol.,* **40**, 1151-1185.

Deschamps M. (1995) - Le magmatisme du Champ-du-Feu (Vosges septentrionales). Caractérisation et signification géotectonique. *Bull. Acad. Soc. Lorraine Sciences,* **34**, 131-149.

Dezayes C., Villemin T., Genter A., Traineau H., Angelier J. (1995) - Analysis of fractures in boreholes of the Hot Dry Rock project at Soultz-sous-Forêts (Rhine Graben, France). *Scient. Drilling,* **5**, 31-41.

Dezayes C., Villemin T., Genter A., Angelier J. (1996) - Origine et signification des fractures de relaxation dans les carottes de granite du forage EPS1 (Soultz-sous-Forêts, graben du Rhin). *C.R. Acad. Sci. Paris,* **323**, 333-340.

Dezayes C., Villemin T., Pêcher A. (2000) - Microfracture pattern compared to core-scale fractures in the borehole of Soultz-sous-Forêts granite, Rhine Graben, France. *J. Struct. Geol.,* **22**, 723-733.

Dias G., Leterrier J. (1994) - The genesis of felsic-mafic plutonic associations: a Sr and Nd isotopic study of the Hercynian Braga granitoid massif (Northern Portugal). *Lithos,* **32,** 207-223.

Didier J., Barbarin B. (1991) - The granites and their enclaves. *Developments in Petrology,* vol. **3**, Elsevier, Amsterdam.

Droop G.T.R. (1987) - A general equation for estimating Fe^{3+} concentration in ferromagnesian silicates and oxides from microprobe analyses, using stoichiometric data. *Mineral. Magazine,* **51**, 431-435.

Edel J.B., Weber K. (1995) - Cadomian terranes, wrench faulting and thrusting in the Central Europe Variscides: geophysical and geological evidence. *Geol. Rundsch.,* **84**, 412-432.

Elsass P., Aquilina L., Beauce A., Benderitter Y., Genter A., Pauwels H. (1995) - Deep structures of the Soultz-sous-Forêts HDR site. Paper presented at the World Geothermal Congress, Florence, Italy.

Evensen N.M., Hamilton P.J., O'Nions R.K. (1978) - Rare-earth abundances in chondritic meteorites. *Geochim. Cosmochim. Acta,* **42**, 1199-1212.

Faure M., Leloix Ch., Roig J.Y. (1997) - L'évolution polycyclique de la chaîne hercynienne. *Bull. Soc. géol. France,* **168,** 695-705.

Flöttmann Th., Oncken O. (1992) - Constraints on the evolution of the Mid German Crystalline Rise - a study of outcrops west of the river Rhine. *Geol. Rundsch.,* **81**, 515-543.

Foley S.F., Venturelli G., Green D.H., Toscani L. (1987) - The ultrapotassic rocks: characteristics, classification and constraints to petrogenetic models. *Earth Sci. Reviews*, **24**, 81-134.

Franke W. (1989a) - Tectonostratigraphic units in the Variscan belt of Central Europe. *In:* D.R. Dallmeyer (ed.), *Geol. Soc. Amer. Spec. Pap.,* **230**, 67-90.

Franke W. (1989b) - Variscan plate tectonics in Central Europe. Current ideas and open questions. *Tectonophysics,* **169**, 221-228.

Franke W., Dallmeyer R.D., Weber K. (1995) - Geodynamic evolution. *In:* Pre-Permian geology of Central and Eastern Europe, D.R. Dallmeyer *et al.* (eds.), Springer Verlag, Berlin, Heidelberg, 579-593.

Gagny C., Cuney M. (1997) - Pétrologie structurale du « massif » de Charroux-Civray. Conséquence d'une mise en place dans un affrontement de plaques en transpression. *In*: Atlas des posters des journées scientifiques de Poitiers, 13-14 October 1997, CNRS and ANDRA (eds.), 20-22.

Genter A., Traineau H. (1992) - Borehole EPS-1, Alsace, France: preliminary geological results from granite core analyses for Hot Dry Rock research. *Scient. Drilling,* **3**, 205-214.

Genter A., Traineau H., Dezayes C., Elsass P., Ledésert B., Meunier A., Villemin T. (1995) - Fracture analysis and reservoir characterization of the granitic basement in the HDR Soultz project (France). *Geotherm. Sci. Tech.,* **4,** 189-214.

Gérard A., Kappelmeyer O. (1987) - The Soultz-sous-Forêts project and its specific characteristics with respect to the present state of experiments with HDR. *Geothermics,* **16**, 39-399.

Gradstein F.M., Odd J. (1997) - A Phanerozoic time scale. *Episodes,* **19**, 3-5.

Haggerty S.E. (1976) - Opaque mineral oxides in terrestrial igneous rocks. *In:* Rumble D. (ed.), Oxide Minerals. *Min. Soc. Am., Short Courses,* Notes, **3**, chap. 8.

Hellmann K.H., Lippolt H.J., Todt W. (1982) - Interpretation der Kalium-Argon-Alter eines Odenwälder Granodioritporphyrit Ganges und seiner Nebengesteine. *Aufschluss, Heidelberg,* **33**, 155-164.

Henk A. (1995) - Late Variscan exhumation histories of the southern Rheno-hercynian zone and western Mid-German Crystalline Rise: results from thermal modeling. *Geol. Rundsch.,* **84**, 578-590.

Hess J.C., Lippolt H.J., Kober B. (1995) - The age of the Kagenfels granite (northern Vosges) and its bearing on the intrusion scheme of the late Variscan granitoids. *Geol. Rundsch.,* **84**, 568-577.

Holden P., Halliday A.N., Stephens W.E. (1987) - Neodymium and strontium isotope content of microdiorite enclaves points to mantle input to granitoid production. *Nature, G.B.,* **330**, 53-56.

Holland T., Blundy J. (1994) - Non-ideal interactions in calcic amphiboles and their bearing on amphibole-plagioclase thermometry. *Contrib. Mineral. Petrol.,* **116**, 433-447.

Kappelmeyer O., Gérard A., Schloemer W., Ferrandes R., Rummel F., Benderitter Y. (1991) - European HDR project at Soultz-sous-Forêts general presentation. *Geotherm. Sci. Technol.,* **2**, 263-289.

Kirsch H., Kober B., Lippolt H.J. (1988) - Age of intrusion and rapid cooling of the Frankenstein gabbro (Odenwald, SW-Germany) evidenced by $^{40}Ar/^{39}Ar$ and single zircon $^{207}Pb/^{206}Pb$ measurements. *Geol. Rundsch.,* **77**, 693-711.

Krohe A. (1991) - Emplacement of synkinematic plutons in the Variscan Odenwald (Germany) controlled by transtensional tectonics. *Geol. Rundschau,* **80**, 391-402.

Langer C., Altherr R., Hegner E., Satir M., Henjes-Kunst F. (1995) - Moldanubian granitoids of the Vosges: evidence for diverse crustal and mantle sources. *Terra, Abstr.,* **7**, 299.

Langmuir C.H. (1989) - Geochemical consequences of in-situ crystallization. *Nature, G.B.,* **340**, 199-205.

Leake B.E. *et al.* (1997) - Nomenclature of amphiboles: report of the Subcommittee on amphiboles of the International Mineralogical Association Commission on New Minerals and Mineral Names. *Mineral. Magazine,* **61**, 295-321.

Ledésert B., Berger G, Meunier A., Genter A., Bouchet A. (1999) - Diagenetic-type reactions related to hydrothermal alteration in the Soultz-sous-Forêts granite, France. *Eur. J. Miner.,* **11**, 731-741.

Lo C.H., Onstott T.C. (1989) - ^{39}Ar recoil artefacts in chloritized biotite. *Geochim. Cosmochim. Acta,* **53**, 2697-2711.

Michael P.J. (1984) - Chemical differentiation of the Cordillera Paine granite, southern Chile, by in-situ fractional crystallization. *Contrib. Mineral. Petrol.,* **87**, 179-195.

Mittlefieldt D.W., Miller C.F. (1983) - Geochemistry of the Sweetwater Wash pluton, California: implications for "anomalous" trace-element behavior during differentiation of felsic magmas. *Geochim. Cosmochim. Acta,* **47**, 109-124.

Monier G. (1987) - Cristallochimie des micas des leucogranites. Nouvelles données expérimentales et applications pétrologiques. *Géol. Géochim. Uranium,* Mém. **14**, 345 p., Nancy, Centre Recherches Géologie Uranium, Vandoeuvre, France.

Nachit H., Razafimahefa N., Stussi J.M., Carron J.L. (1985) - Composition chimique des biotites et typologie magmatique des granitoïdes. *C.R. Acad. Sci., Fr.,* **301**, 813-818.

Naney M.T. (1983) - Phase equilibria of rock-forming ferromagnesian silicates in granitic systems. *Am. J. Sci.,* **283**, 993-1033.

Neiva A.M.R. (1981) - Geochemistry of hybrid granitoid rocks and of their biotites from central northern Portugal and their petrogenesis. *Lithos,* **14**, 149-163.

Oncken O. (1997) - Transformation of a magmatic arc and an orogenic root during oblique collision and its consequences for the evolution of the European Variscides (Mid-German Crystalline Rise). *Geol. Rundsch.,* **86**, 2-20.

Pagel M., Leterrier J. (1980) - The subalkaline potassic magmatism of the Ballons massif Southern Vosges, France: shoshonitic affinities. *Lithos,* **1**, 1-10.

Pastier P., Sabourdy G. (1990) - Essai de caractérisation des granites limousins par l'étude cristallochimique des biotites. *C.R. Acad. Sci., Fr.,* **311**, 345-348.

Paterson B.A., Stephens W.E. (1992) - Kinetically induced compositional zoning in titanite: implications for accessory-phase/melt partitioning of trace elements. *Contrib. Mineral. Petrol.,* **109**, 373-385.

Patino-Douce A.E. (1993) - Titanium substitution in biotite: an empirical model with applications to thermometry, O2 and H2O barometries, and consequences for biotite stability. *Chem. Geol.,* **108**, 133-162.

Patino-Douce A.E., Beard J.S. (1995) - Dehydration-melting of biotite gneiss and quartz amphibolite from 3 to 15 kbar. *J. Petrol.,* **36**, 707-738.

Peccerillo A., Taylor S.R. (1976) - Geochemistry of Eocene calc-alkaline volcanic rocks from the Kastamonu area, northern Turkey. *Contrib. Mineral. Petrol.,* **58**, 63-81.